

Autonomous Underwater Vehicle Trajectory Tracking Digital Control



Alex Khair and Justin Hart
ME 397: Digital Control

1 Table of Contents

2	Introduction.....	5
2.1	Objective	5
2.2	Scope	5
3	Reference Frame Definitions and Transformations.....	6
3.1	Reference Frames	6
3.1.1	NED (North, East, Down) Frame (N).....	6
3.1.2	Body Frame (B)	7
3.1.3	Flow Axes Frame.....	7
3.2	Transformations and Relationships.....	7
3.2.1	Control Point and Center of Gravity	7
3.2.2	NED to Body.....	8
3.2.3	Flow to Body.....	9
4	Plant Model.....	10
4.1	Ocean Currents.....	11
4.2	AUV Shape	11
4.3	Rigid Body Terms	12
4.4	Added Mass Terms [2].....	13
4.5	Hydrostatic Terms	15
4.6	Loss Terms	16
4.6.1	Linear Viscous Drag	16
4.6.2	Drag Force, Lift Force	16
4.6.3	Cross Flow Drag	18
4.6.4	Rudder Sway Force/Moment	19
4.6.5	Stern Plane Heave Force/Moment	19
4.7	Plant Model in Terms of Absolute Velocity	20
5	Emulation Setup.....	21
5.1	State Space Representation	23
5.2	Inputs Discussion	23
5.3	PID controllers	25
5.4	MIMO to SISO Discussion	25
6	Results.....	26
6.1	Simulation Parameters.....	26

6.2	Sampling Time Analysis	27
6.3	Trajectory 1, Fast Current	31
6.4	Trajectory 2, Fast Current	34
6.5	Trajectory 3, Fast Current	36
6.6	Trajectory 1, Non-Uniform Density.....	38
7	Conclusions/Future Work	41
8	References.....	42
	Appendix A: Acronyms List.....	42
	Appendix B: Variable List.....	43
	Appendix C: Miscellaneous Derivations	45

Figure 1: NED frame definition [1]	6
Figure 2: Body frame definition	7
Figure 3: Vector relationships between frames and points of interest.....	8
Figure 4: Body and Flow axes relationship	9
Figure 5: Prolate spheroid representation of AUV positioned in the body frame	12
Figure 6: Hydrostatic forces.....	15
Figure 7: Drag and lift force schematic, relative to angle of attack and flow direction [3].....	17
Figure 8: Hoerner Curve	19
Figure 9: System Block Diagram.....	21
Figure 10: Reference Inputs/Trajectories.....	22
Figure 11: Controllable inputs	24
Figure 12: Sampling time analysis. Sampling time = .05 seconds (20 Hz), yaw trajectory 1, .5 m/sec current speed, fixed sideslip angle.....	29
Figure 13:Sampling time analysis. Sampling time = .15 seconds (6.67 Hz), yaw trajectory 1, .5 m/sec current speed, fixed sideslip angle.....	31
Figure 14: Trajectory 1 Tracking. Sampling time = .05 seconds (20 Hz), yaw trajectory 1, 1.5 m/sec current speed, fixed sideslip angle.....	33
Figure 15: Trajectory 2 Tracking. Sampling time = .05 seconds (20 Hz), yaw trajectory 2, 1.5 m/sec current speed, fixed sideslip angle.....	36
Figure 16:Trajectory 3 Tracking. Sampling time = .05 seconds (20 Hz), yaw trajectory 3, 1.5 m/sec current speed, fixed sideslip angle.....	38
Figure 17:Nonuniform Density. Sampling time = .05 seconds (20 Hz), yaw trajectory 1, .5 m/sec current speed, fixed sideslip angle	41

2 Introduction

Autonomous underwater vehicles (AUVs) are unmanned underwater robots that operate independently from humans. As technological improvements advance the usefulness of AUVs, they are being rapidly implemented into industries that can benefit from their small size, their autonomy, and the vast array of sensors that can be outfitted onto the vessel.

Three industries that are beginning to utilize AUVs include oil and gas [5], defense [6], and oceanographic research [4]. In oil and gas, AUVs are being used to map the seafloor prior to constructing subsea infrastructure, saving time and money vs. traditional methods. They can also reach greater depths than previous methods allowed. In the defense industry, AUVs can be used as mine hunters, for surveillance and reconnaissance, for anti-submarine warfare, and for payload delivery. The greatest benefit in the defense industry is the autonomy provided which increases the safety of personnel that would otherwise be placed in harm's way. For oceanographic research, AUVs can be used for data collection and sampling, and lowers personnel costs compared with current methods. AUVs can reach shallower water than most research vessels and deeper water than human divers.

As these industries and more apply the benefits of AUVs to their work, and as more uses are discovered, current research being completed to improve performance includes optimization and development of models and controllers. This includes PID pole placement [1], nonlinear [7] and path-following [8] control as well as model predictive control [9]. This project focuses on developing a digital controller for trajectory tracking of an AUV. The AUV model used is the REMUS 100, developed by Woods Hole Oceanographic institute.

2.1 Objective

There are two main objectives of this project. The first is to replicate the REMUS 100 plant model as presented in [1] in order to study trajectory tracking of an AUV. This is done by first deriving the six degree of freedom plant model, and then utilizing PID controllers to control the three control inputs into the AUV. Then the system (controllers plus plant model) can be emulated in discrete time.

The second objective is to investigate the system performance qualitatively. To do this we can look at the sampling rate effect on system stability, assess the ability of the controllers to track different trajectories, and analyze the robustness of the system to disturbances.

2.2 Scope

As mentioned in the introduction, the plant model derived is for a REMUS 100 AUV. The body of the AUV will be modeled as a prolate spheroid and the motor model relating control inputs to force in the x-direction has been simplified for this project.

The disturbance input into the system is the ocean current which will be assumed to be horizontal and irrotational with a constant velocity. What will be varied is the current speed and horizontal angle of the current relative to the heading of the AUV. The two current speeds used are 0.5 m/s, which is the average ocean surface current speed [10], and 1.8 m/s, which is the average speed of

the gulf stream [11], one of the fastest ocean currents. Vertical currents are not included in the simulation in order to simplify the model.

Three different trajectories are simulated, varying in complexity in order to test the controller's ability to track. The first is a ramp to a constant yaw angle, the second is a sine wave yaw angle, and the third is a constantly increasing yaw angle.

The trajectories are specified in terms of yaw angles, cartesian coordinate tracking requires additional relationships between the states and the reference input, this is out of scope of this project.

A motor model converting the three controllable inputs of the AUV to forward thrust is out of scope of this project, a general relationship between them is assumed based on information taken from our reference sources.

3 Reference Frame Definitions and Transformations

3.1 Reference Frames

There are few reference frames of interest when describing the position of an AUV.

3.1.1 NED (North, East, Down) Frame (N)

The NED reference frame is defined as the plane tangent to the surface of the earth, it moves with the marine craft.

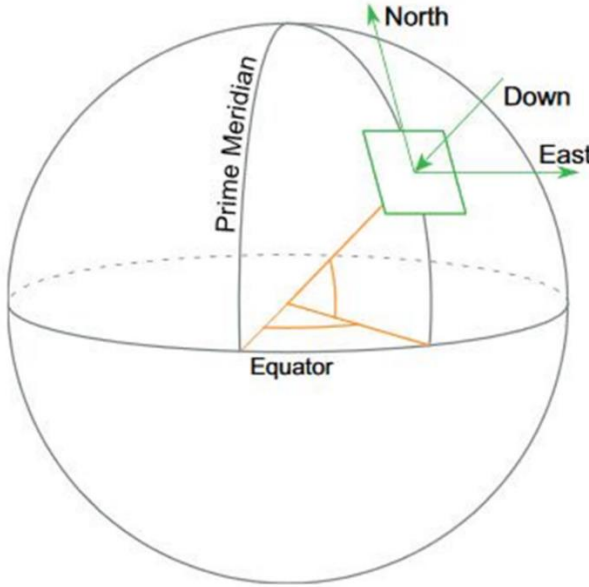


Figure 1: NED frame definition [1]

The flat earth navigation assumption states: For a marine craft moving in an area of approximately constant longitude and latitude (local area), the NED frame is inertial. This assumption allows for application of Newton's laws within the frame and will be used throughout subsequent analysis.

3.1.2 Body Frame (B)

The body frame is fixed to the marine craft, its origin (CO) is located at the geometric middle of the craft.

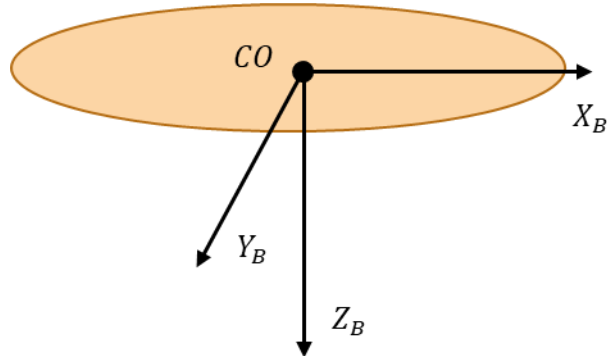


Figure 2: Body frame definition

x_b – longitudinal axis, y_b – transversal axis, z_b – normal axis

3.1.3 Flow Axes Frame

Flow axes are used to express hydrodynamic data. The x_{flow} axis is parallel to the freestream flow (the water in a region where pressure, temperature, and relative velocity are unaffected by the movement of a marine craft through it). The z_{flow} axis points downward, like the z_b axis but rotates to remain perpendicular to the x_{flow} flow axis. The y_{flow} completes the right-handed coordinate system.

This reference frame is convenient for specifying the ocean currents in, computing the hydrodynamic lift force (which is, by definition, perpendicular to relative flow) and the hydrodynamic drag force (which is, by definition, parallel to relative flow).

3.2 Transformations and Relationships

3.2.1 Control Point and Center of Gravity

The body frame is related to the inertial NED frame through the vector $\vec{r}_{B/N}$ which originates at the origin of the NED frame and terminates at the origin of the body frame.

The center of gravity (CG) of the marine craft is related to the NED frame through the vector $\vec{r}_{G/N}$ which originates at the origin of the NED frame and terminates at CG.

CO is related to CG through the vector \vec{r}_G which originates at CO and terminates at CG.

Figure 3 is a visual representation of these relationships.

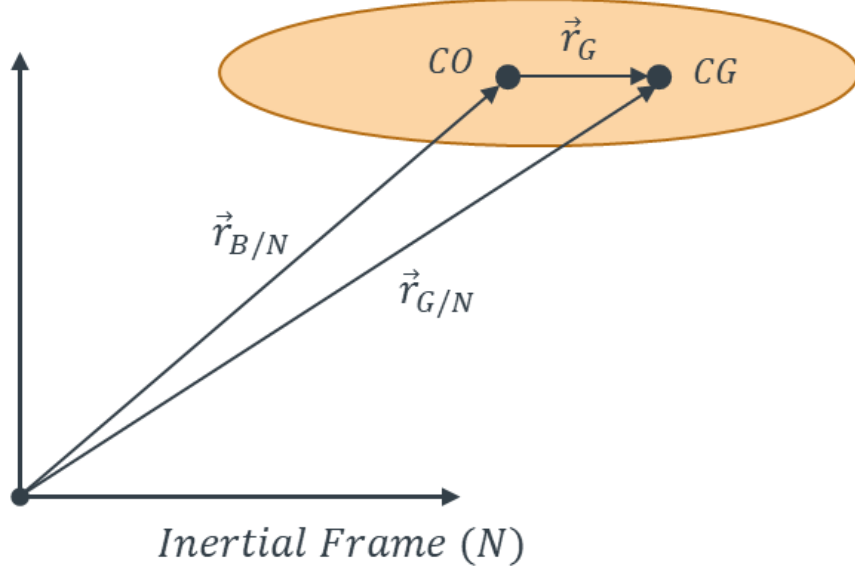


Figure 3: Vector relationships between frames and points of interest

3.2.2 NED to Body

Consider the general rotation matrices for an angle counterclockwise about their respective axes.

$$R_x(\varphi) = \begin{bmatrix} 1 & 0 & 0 \\ 0 & \cos \varphi & -\sin \varphi \\ 0 & \sin \varphi & \cos \varphi \end{bmatrix}, \quad R_y(\theta) = \begin{bmatrix} \cos \theta & 0 & \sin \theta \\ 0 & 1 & 0 \\ -\sin \theta & 0 & \cos \theta \end{bmatrix}, \quad \text{Eqn. 3-1}$$

$$R_z(\psi) = \begin{bmatrix} \cos \psi & -\sin \psi & 0 \\ \sin \psi & \cos \psi & 0 \\ 0 & 0 & 1 \end{bmatrix}$$

The rotation matrix from body to NED frame is given by

$$R_B^N = R_z(\psi)R_y(\theta)R_x(\varphi) \quad \text{Eqn. 3-2}$$

The rotation matrix from NED to body is the inverse of Eqn. 3-2

$$R_N^B = (R_B^N)^{-1} = R_x(\varphi)^T R_y(\theta)^T R_z(\psi)^T \quad \text{Eqn. 3-3}$$

To transform the angular velocity from the NED to body frame. Consider the vector $x(t)$ which defines the position of any point in a rigid body undergoing rotation. The motion of $x(t)$ is described by using the time dependent symmetric rotation $R(t)$

$$x(t) = R(t)x(0) \quad \text{Eqn. 3-4}$$

The velocity of this point in the body is

$$\frac{dx(t)}{dt} = \dot{x}(t) = \dot{R}(t)x(0) = \dot{R}(t)R^{-1}x(t) = \dot{R}(t)R^T x(t) \quad \text{Eqn. 3-5}$$

The angular velocity, ω , of a general vector x is given by

$$\dot{x} = \frac{dx}{dt} = \omega \times x = S(\omega)x \quad \text{Eqn. 3-6}$$

Where $S(\lambda)$ is the skew symmetric cross product operator

$$S(\lambda) = -S^T(\lambda) = \begin{bmatrix} 0 & -\lambda_3 & \lambda_2 \\ \lambda_3 & 0 & -\lambda_1 \\ -\lambda_2 & \lambda_1 & 0 \end{bmatrix} \quad \text{Eqn. 3-7}$$

A useful property of the S operator

$$S^T(a)b = -S(a)b = S(b)a \quad \text{Eqn. 3-8}$$

Relating this back to the rotation of interest, R_B^N , the angular velocity of the basis not rotating with the body ω_N can be found from

$$S(\omega_N) = \dot{R}_B^N (R_B^N)^T = \begin{bmatrix} 0 & -\omega_{N3} & \omega_{N2} \\ \omega_{N3} & 0 & -\omega_{N1} \\ -\omega_{N2} & \omega_{N1} & 0 \end{bmatrix} \quad \text{Eqn. 3-9}$$

To transform angular velocity from the NED to the body frame

$$\omega_B = (R_B^N)^T \omega_N = T_N^B \omega_N$$

where $T_N^B = \begin{bmatrix} 1 & 0 & -\sin \theta \\ 0 & \cos \varphi & \cos \theta \sin \varphi \\ 0 & -\sin \varphi & \cos \theta \cos \varphi \end{bmatrix}$

$$\quad \text{Eqn. 3-10}$$

3.2.3 Flow to Body

The flow axes are first rotated by a negative sideslip angle, $-\beta$, about the z_b axis and subsequently rotated by the angle of attack, α , about the y_b axis.

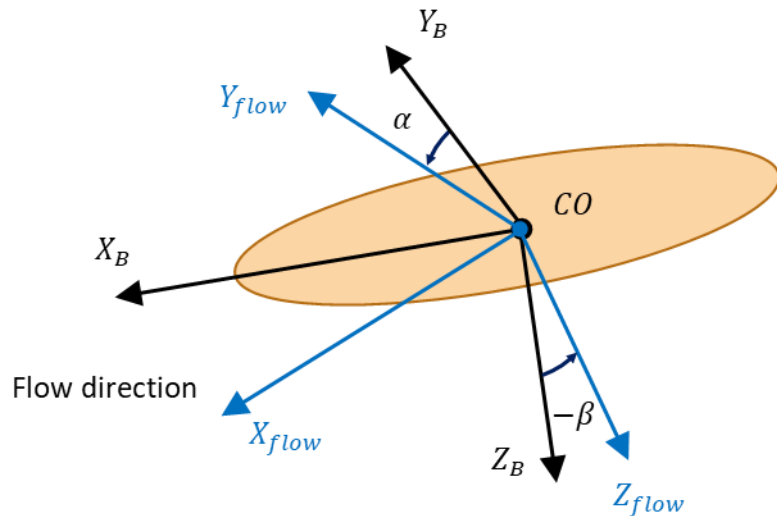


Figure 4: Body and Flow axes relationship

Mathematically the relationship between the flow and body frame is given by the following.

Rotation from body to flow:

$$R_B^{Flow} = R_z(-\beta)R_y(\alpha) = R_z(\beta)^T R_y(\alpha) \quad \text{Eqn. 3-11}$$

Rotation from flow to body:

$$R_{Flow}^B = R_y(\alpha)^T R_z(\beta) \quad \text{Eqn. 3-12}$$

Where the rotation matrices about an axis are given by Eqn. 3-1

4 Plant Model

The equation of motion of an underwater vehicle is given by:

$$M_{RB}\dot{v}_G^B + C_{RB}(v_G^B)v_G^B + M_A\dot{v}_{rel}^B + C_A(v_{rel}^B)v_{rel}^B + D(v_{rel}^B)v_{rel}^B + g(\eta^N) = \tau_{Input} + \tau_{Current} + \tau_{DragLift} + \tau_{CrossFlowDrag} \quad \text{Eqn. 4-1}$$

Where:

- M_{RB} is the rigid body mass matrix

- v_G^B is the generalized velocity vector $\begin{bmatrix} u \\ v \\ w \\ p \\ q \\ r \end{bmatrix} = \begin{bmatrix} v^B \\ \omega_{B/N}^B \end{bmatrix} = \begin{bmatrix} \text{Linear velocity in } x \\ \text{Linear velocity in } y \\ \text{Linear velocity in } z \\ \text{Angular velocity about } x \\ \text{Angular velocity about } y \\ \text{Angular velocity about } z \end{bmatrix}$

- C_{RB} is the rigid body Coriolis and centripetal matrix due to rotation of B about N
- M_A is the added mass matrix due to displacement of the surrounding fluid
- v_{rel}^B is the relative (to the ocean currents) velocity vector in the body frame
- C_A is the added Coriolis and centripetal matrix due to displacement of the surrounding fluid
- D is the linear damping matrix
- g is the gravitational and buoyancy forces and moments

- η^N is the generalized position vector in NED frame $\eta^N = \begin{bmatrix} x \\ y \\ z \\ \phi \\ \theta \\ \psi \end{bmatrix} = \begin{bmatrix} x \text{ Position} \\ y \text{ Position} \\ z \text{ Position} \\ \text{Angle about } x \\ \text{Angle about } y \\ \text{Angle about } z \end{bmatrix}$

- τ_{Input} is the control forces and moments
- $\tau_{Current}$ is the forces and moments induced by the ocean currents
- $\tau_{DragLift}$ is the hydrodynamic lift/drag forces
- $\tau_{CrossFlowDrag}$ is the hydrodynamic cross flow drag terms

4.1 Ocean Currents

The ocean currents are assumed to be irrotational (no rotational component to the flow) and constant. In the flow reference frame, the speed of the current is denoted by V_c . By definition of the flow frame (Section 3.1.3), the current acts along the x_{Flow} axis. The linear current expressed in the body frame is given by.

$$v_c^B = R_{Flow}^B \begin{bmatrix} V_c \\ 0 \\ 0 \end{bmatrix} \quad \text{Eqn. 4-2}$$

Where the rotation matrix R_{Flow}^B is given by Eqn. 3-12.

Therefore, the relative velocity v_{rel} is given by

$$v_{rel}^B = \begin{bmatrix} v_G^B - v_c^B \\ \omega_{B/N}^B \end{bmatrix} \quad \text{Eqn. 4-3}$$

Where v^B is the linear velocity vector in the body frame and $\omega_{B/N}^B$ is the angular velocity vector of the body frame relative to the NED frame in the body frame.

An irrotational constant ocean current in the NED frame, v_c^N , is defined by

$$\dot{v}_c^N = \frac{d}{dt} (R_B^N v_c^B) = \dot{R}_B^N v_c^B + R_B^N \dot{v}_c^B = 0 \quad \text{Eqn. 4-4}$$

where

$$\dot{R}_B^N = R_B^N S(\omega_{B/N}^B)$$

From Eqn. 4-4 it can be seen that

$$\begin{aligned} R_B^N S(\omega_{B/N}^B) v_c^B + R_B^N \dot{v}_c^B &= 0 \\ \rightarrow S(\omega_{B/N}^B) v_c^B + \dot{v}_c^B &= 0 \\ \rightarrow \dot{v}_c^B &= -S(\omega_{B/N}^B) v_c^B \end{aligned} \quad \text{Eqn. 4-5}$$

This observation will be important in Section 4.7

4.2 AUV Shape

The AUV is represented by a prolate spheroid (a spheroid with 2 semi axes of equal length and one longer semi axis) with its center at the origin of the body frame. Given by the equation

$$\frac{x^2}{a^2} + \frac{y^2}{b^2} + \frac{z^2}{c^2} = 1$$

Where $b = c$, and $a > b$

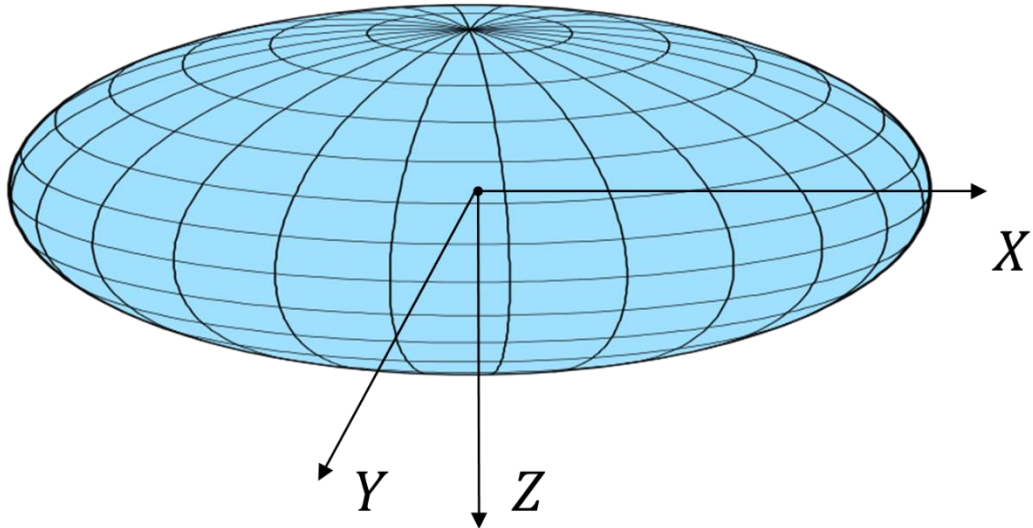


Figure 5: Prolate spheroid representation of AUV positioned in the body frame

The spheroid is sectioned off into two pieces, each of a unique density; uniform density is assumed across each piece. This allows for the user to specify differing material compositions for the front end which may contain more of the electronics and a rear end which will consist of the motor/propellor assembly and fuel source (in this case the battery).

There are two points of interest within the spheroid:

First, the centroid of a section of the spheroid, this is the location of CO, the origin of the body frame. The buoyancy force acts upwards at the centroid of the spheroid. The centroid is given by:

$$\bar{x} = \frac{\int x \, dV}{\int dV}, \quad \bar{z} = 0, \quad \bar{y} = 0 \quad \text{Eqn. 4-6}$$

The derivation of \bar{x} can be found in Appendix C: Miscellaneous Derivations

Second, the center of gravity of the total spheroid. This is the point at which the center of gravity acts upon. Due to the nonuniform density of the object (2 separate sections of uniform density), it will be shifted from the centroid of the spheroid. The center of gravity is then given by

$$\bar{x}_{CG} = \frac{\sum m_i \bar{x}_i}{\sum m_i}, \quad \bar{y}_{CG} = \frac{\sum m_i \bar{y}_i}{\sum m_i}, \quad \bar{z}_{CG} = \frac{\sum m_i \bar{z}_i}{\sum m_i} \quad \text{Eqn. 4-7}$$

The derivation of the center of gravity can be found in Appendix C: Miscellaneous Derivations

4.3 Rigid Body Terms

Our first consideration in the derivation of the plant model are the rigid body terms. The object has mass, that mass is capable of rotation. As such, the rigid body mass and Coriolis-centripetal

matrices are derived from the linear and angular momentum of the center of gravity of the AUV, CG, with respect to the inertial frame, N.

The Newton-Euler equations of motion about CG are given by

$$\begin{bmatrix} mI_{3x3} & 0_{3x3} \\ 0_{3x3} & I_G \end{bmatrix} \begin{bmatrix} \dot{v}_{G/N}^B \\ \dot{\omega}_{B/N}^B \end{bmatrix} + \begin{bmatrix} mS(\omega_{B/N}^B) & 0_{3x3} \\ 0_{3x3} & -S(I_G \omega_{B/N}^B) \end{bmatrix} \begin{bmatrix} v_{G/N}^B \\ \omega_{B/N}^B \end{bmatrix} = \begin{bmatrix} f_G^B \\ m_G^B \end{bmatrix} \quad \text{Eqn. 4-8}$$

where

$$M_{RB}^{CG} = \begin{bmatrix} mI_{3x3} & 0_{3x3} \\ 0_{3x3} & I_G \end{bmatrix}, \quad C_{RB}^{CG} = \begin{bmatrix} mS(\omega_{B/N}^B) & 0_{3x3} \\ 0_{3x3} & -S(I_G \omega_{B/N}^B) \end{bmatrix}$$

About the control point, CO, these matrices are given by

$$\begin{aligned} M_{RB}^{CO} &= \begin{bmatrix} mI_{3x3} & -mS(r_G^B) \\ mS(r_G^B) & I_G - mS^2(r_G^B) \end{bmatrix} \\ C_{RB}^{CO} &= \begin{bmatrix} mS(\omega_{B/N}^B) & -mS(\omega_{B/N}^B)S(r_G^B) \\ mS(r_G^B)S(\omega_{B/N}^B) & mS(r_G^B)S(\omega_{B/N}^B)S^T(r_G^B) - S(I_G \omega_{B/N}^B) \end{bmatrix} \end{aligned} \quad \text{Eqn. 4-9}$$

Where the mass moment of inertia matrix, I_G , is given by

$$I_G = \begin{bmatrix} I_x & -I_{xy} & -I_{xz} \\ -I_{yx} & I_y & -I_{yz} \\ -I_{zx} & -I_{zy} & I_z \end{bmatrix} \quad \text{Eqn. 4-10}$$

For a step-by-step derivation of these matrices from the conservation of linear and angular momentum, see Appendix C: Miscellaneous Derivations.

4.4 Added Mass Terms [2]

Motion of a body in an otherwise stationary fluid imparts kinetic energy onto the fluid that it would not possess if the body was not in motion. To pass through the fluid the body forces the fluid to move aside and close in behind it. The added mass terms in the overall equation of motion, Eqn. 4-1, accounts for this effect.

In general, the added mass matrix is given by:

$$M_A = \begin{bmatrix} X_{\dot{u}} & X_{\dot{v}} & X_{\dot{w}} & X_{\dot{p}} & X_{\dot{q}} & X_{\dot{r}} \\ Y_{\dot{u}} & Y_{\dot{v}} & Y_{\dot{w}} & Y_{\dot{p}} & Y_{\dot{q}} & Y_{\dot{r}} \\ Z_{\dot{u}} & Z_{\dot{v}} & Z_{\dot{w}} & Z_{\dot{p}} & Z_{\dot{q}} & Z_{\dot{r}} \\ K_{\dot{u}} & K_{\dot{v}} & K_{\dot{w}} & K_{\dot{p}} & K_{\dot{q}} & K_{\dot{r}} \\ M_{\dot{u}} & M_{\dot{v}} & M_{\dot{w}} & M_{\dot{p}} & M_{\dot{q}} & M_{\dot{r}} \\ N_{\dot{u}} & N_{\dot{v}} & N_{\dot{w}} & N_{\dot{p}} & N_{\dot{q}} & N_{\dot{r}} \end{bmatrix} \quad \text{Eqn. 4-11}$$

For an ellipsoid

$$\begin{aligned}
X_{\dot{u}} &= -\frac{\alpha_0}{2-a_0} \left(\frac{4}{3} \pi \rho abc \right), & Y_{\dot{v}} &= -\frac{\beta_0}{2-\beta_0} \left(\frac{4}{3} \pi \rho abc \right), \\
Z_{\dot{w}} &= -\frac{\gamma_0}{2-\gamma_0} \left(\frac{4}{3} \pi \rho abc \right) \\
K_{\dot{p}} &= -\frac{1}{5} \frac{(b^2 - c^2)^2 (\gamma_0 - \beta_0)}{2(b^2 - c^2) + (b^2 + c^2)(\beta_0 - \gamma_0)} \left(\frac{4}{3} \pi \rho abc \right) \\
M_{\dot{q}} &= -\frac{1}{5} \frac{(c^2 - a^2)^2 (\alpha_0 - \gamma_0)}{2(c^2 - a^2) + (c^2 + a^2)(\gamma_0 - \alpha_0)} \left(\frac{4}{3} \pi \rho abc \right) \\
N_{\dot{r}} &= -\frac{1}{5} \frac{(a^2 - b^2)^2 (\beta_0 - \alpha_0)}{2(a^2 - b^2) + (a^2 + b^2)(\alpha_0 - \beta_0)} \left(\frac{4}{3} \pi \rho abc \right) \\
X_{\dot{v}} = X_{\dot{w}} = X_{\dot{p}} = X_{\dot{q}} = X_{\dot{r}} &= Y_{\dot{w}} = Y_{\dot{p}} = Y_{\dot{q}} = Y_{\dot{r}} = 0 \\
Z_{\dot{p}} = Z_{\dot{q}} = Z_{\dot{r}} = K_{\dot{q}} = K_{\dot{r}} = M_{\dot{r}} &= 0
\end{aligned} \tag{Eqn. 4-12}$$

For a prolate spheroid where the major axis is along the y axis ($b = c$, $a > b$). This simplifies to

$$M_A = \begin{bmatrix} X_{\dot{u}} & 0 & 0 & 0 & 0 & 0 \\ 0 & Y_{\dot{v}} & 0 & 0 & 0 & 0 \\ 0 & 0 & Z_{\dot{w}} & 0 & 0 & 0 \\ 0 & 0 & 0 & 0 & 0 & 0 \\ 0 & 0 & 0 & 0 & M_{\dot{q}} & 0 \\ 0 & 0 & 0 & 0 & 0 & N_{\dot{r}} \end{bmatrix}$$

where

$$\begin{aligned}
X_{\dot{u}} = Z_{\dot{w}} &= -\frac{\alpha_0}{2-a_0} \left(\frac{4}{3} \pi \rho ab^2 \right), & Y_{\dot{v}} &= -\frac{\beta_0}{2-\beta_0} \left(\frac{4}{3} \pi \rho ab^2 \right) \\
N_{\dot{r}} = M_{\dot{q}} &= -\frac{1}{5} \frac{(b^2 - a^2)^2 (\alpha_0 - \beta_0)}{2(b^2 - a^2) + (b^2 + a^2)(\beta_0 - \alpha_0)} \left(\frac{4}{3} \pi \rho ab^2 \right)
\end{aligned} \tag{Eqn. 4-13}$$

And

$$\begin{aligned}
e^2 &= 1 - \left(\frac{b}{a} \right)^2 \\
\alpha_0 &= \frac{2(1-e^2)}{e^3} \left(\frac{1}{2} \log \left(\frac{1+e}{1-e} \right) - e \right) \\
\beta_0 &= \gamma_0 = \frac{1}{e^2} - \frac{1-e^2}{2e^3} \log \left(\frac{1+e}{1-e} \right)
\end{aligned}$$

From the added mass matrix, the added Coriolis-centripetal matrix is found through the relationship derived in Eqn. C-31

$$C_A(v_{rel}^B) = \begin{bmatrix} 0_{3x3} & -S(M_{11}v_1 + M_{12}v_2) \\ -S(M_{11}v_1 + M_{12}v_2) & -S(M_{21}v_1 + M_{22}v_2) \end{bmatrix} \tag{Eqn. 4-14}$$

where, $M_A = \begin{bmatrix} M_{11} & M_{12} \\ M_{21} & M_{22} \end{bmatrix}$

4.5 Hydrostatic Terms

There are two hydrostatic forces act on the vehicle:

1. The buoyancy force which acts directly upwards in the NED frame at the center of buoyancy of the craft. Since the craft is symmetric the center of buoyancy is equivalent to CO. The buoyancy force in in the NED frame is given by

$$F_B^N = - \begin{bmatrix} 0 \\ 0 \\ \rho_{water} g V \end{bmatrix} \quad \text{Eqn. 4-15}$$

2. The gravitational force which acts directly downwards on the center of gravity of the craft in the NED frame. This is given by

$$F_G^N = \begin{bmatrix} 0 \\ 0 \\ mg \end{bmatrix} \quad \text{Eqn. 4-16}$$

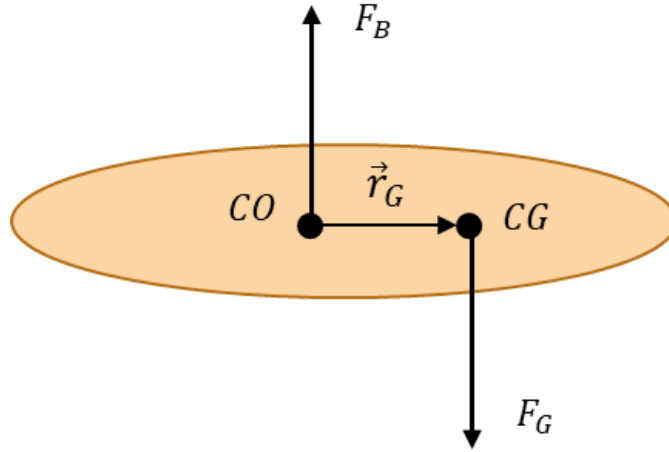


Figure 6: Hydrostatic forces

The restoring force and moment vector in the body frame is

$$\begin{aligned} g(\eta) &= - \left[r_G^B \times F_G^B + r_B^B \times F_B^B \right] \\ &= - \left[r_G^B \times R_N^B(\Theta) (F_G^N + F_B^N) + r_B^B \times R_N^B(\Theta) F_B^N \right] \end{aligned} \quad \text{Eqn. 4-17}$$

Where the rotation matrix from the body to NED frame, $R_N^B(\Theta)$, is given by Eqn. 3-3 and the buoyancy and gravitational forces in the NED frame, F_B^N and F_G^N are given by Eqn. 4-15 and Eqn. 4-16 respectively.

4.6 Loss Terms

4.6.1 Linear Viscous Drag

The equations of motion can be represented in terms of a hydrodynamic mass-damper-spring system. In general, this system varies with the frequencies of the forced oscillations but given that our system is completely submerged under water and not impacted by the motion of the waves, it's frequency dependence can be neglected.

$$A\ddot{\xi} + B\dot{\xi} + C\xi = \tau \quad \text{Eqn. 4-18}$$

Where A is the sum of the rigid body and added mass matrix, B is the damping matrix, and C is the spring stiffness or hydrostatic matrix.

The linear damping matrix D is due to viscous damping and possible skin friction due to laminar boundary layer theory. In general, the motion of an underwater vehicle at high speeds is highly nonlinear and coupled. An assumption that can be made for an AUV only capable of operating at low speeds, for a vehicle that has three planes of symmetry, is that the off-diagonal elements of the D matrix can be neglected.

$$D = - \begin{bmatrix} X_u & 0 & 0 & 0 & 0 & 0 \\ 0 & Y_v & 0 & 0 & 0 & 0 \\ 0 & 0 & Z_w & 0 & 0 & 0 \\ 0 & 0 & 0 & K_p & 0 & 0 \\ 0 & 0 & 0 & 0 & M_q & 0 \\ 0 & 0 & 0 & 0 & 0 & N_r \end{bmatrix} \quad \text{Eqn. 4-19}$$

A common way to define terms in the damping matrix are to select time constants in surge (motions in x_B direction), sway (motions in y_B direction), yaw (rotation about z_B direction)

$$-X_u = D_{11} = \frac{A_{11}}{T_1}, \quad -Y_v = D_{22} = \frac{A_{22}}{T_2}, \quad -N_r = D_{66} = \frac{A_{66}}{T_6} \quad \text{Eqn. 4-20}$$

At high speeds, these terms vanish and are dominated by the quadratic drag and lift forces defined in Sections 4.6.2 and 4.6.3.

To account for the remaining terms in the linear damping matrix, relative damping ratios are specified in roll (rotation about x_B direction), and pitch (rotation about y_B direction)

$$-Z_w = 2\zeta_3\omega_3M_{33}, \quad -K_p = 2\zeta_4\omega_4M_{44}, \quad -M_q = 2\zeta_5\omega_5M_{55} \quad \text{Eqn. 4-21}$$

Where $\omega_i = \sqrt{\frac{C_{ii}}{A_{ii}}}$

Viscous damping in heave (motions in z_B direction D_{33}) is typically added as a constant value, in our case equal to the damping in surge (D_{22}), to increase the damping at the natural frequency ω_3 .

4.6.2 Drag Force, Lift Force

Drag force is the resistance an object moving through a fluid experiences. The force acts in the direction opposite to the object's motion. The shape of the object, S, the density of the fluid,

ρ_{water} , and the relative velocity of the object with respect to the fluid, v_{rel} , contribute to the total drag force.

$$F_{drag} = \frac{1}{2} \rho_{water} v_{rel}^2 S C_D \quad \text{Eqn. 4-22}$$

Lift is exerted by a fluid flowing around an object. This force is exerted perpendicular to the flow direction, X_{Flow} . Similar to the drag force it can be computed as

$$F_{Lift} = \frac{1}{2} \rho_{water} v_{rel}^2 S C_L \quad \text{Eqn. 4-23}$$

In general, these forces are nonlinear, however, for small angles of attack (the angle between a reference line on the object in motion and the fluid flow direction) the flow of the fluid over the object body remains laminar and a linear approximation is accurate enough.

The coefficients of lift, C_L , and drag, C_D , have a dependence on the angle of attack, α , the pitch rate, and the elevator deflection (a component of a craft which affects its pitch). Due to our application of an underwater vehicle rather than an aircraft, we neglect its dependence on the pitch rate as we assume the pitch angle will not vary much. The lift effects of the elevator (or stern plane will be discussed in Section 4.6.5).

Eqn. 4-22 and Eqn. 4-23 can be expressed as

$$F_{drag} = \frac{1}{2} \rho_{water} v_{rel}^2 S (C_{D_0} + C_{D\alpha} \alpha) \quad \text{Eqn. 4-24}$$

$$F_{Lift} = \frac{1}{2} \rho_{water} v_{rel}^2 S (C_{L_0} + C_{L\alpha} \alpha) \quad \text{Eqn. 4-25}$$

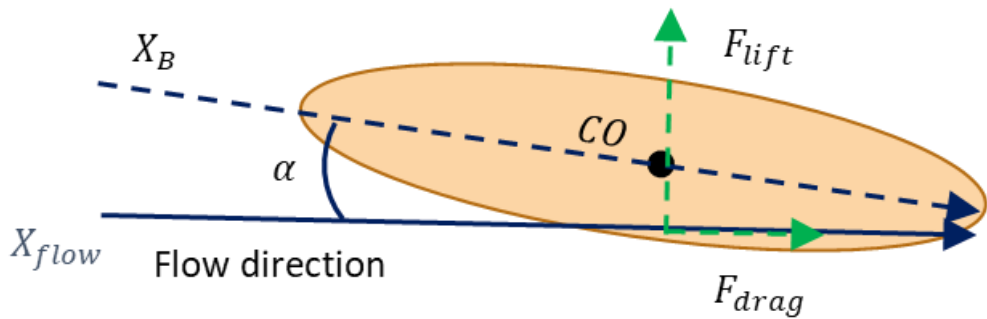


Figure 7: Drag and lift force schematic, relative to angle of attack and flow direction [3]

The linear terms coefficients can be approximated as

$$C_{L\alpha} = \frac{\pi AR}{1 + \sqrt{1 + \left(\frac{AR}{2}\right)^2}} \quad \text{Eqn. 4-26}$$

The aspect ratio, $AR \approx \frac{a^2}{S}$

$$C_D(\alpha) = C_{Dp} + \frac{(C_{L0} + C_{L\alpha}\alpha)^2}{\pi e AR} \quad \text{Eqn. 4-27}$$

The components of drag and lift forces in the body frame can be found through rotating the angle of attack counterclockwise about the Y_B axis

$$\begin{bmatrix} \tau_{DragLift,X_B} \\ \tau_{DragLift,Z_B} \end{bmatrix} = \begin{bmatrix} \cos \alpha & -\sin \alpha \\ \sin \alpha & \cos \alpha \end{bmatrix} \begin{bmatrix} -F_{drag} \\ -F_{lift} \end{bmatrix} = \begin{bmatrix} -F_{drag} \cos \alpha + F_{lift} \sin \alpha \\ -F_{drag} \sin \alpha - F_{lift} \cos \alpha \end{bmatrix} \quad \text{Eqn. 4-28}$$

4.6.3 Cross Flow Drag

Cross flow drag is drag perpendicular to the flow. The expression for computing the various components of the cross-flow drag are given by:

$$Y = -\frac{1}{2} \rho_{water} \int_{-L/2}^{L/2} T(x) C_d^{2D}(x) |v_r + xr_r| (v_r + xr_r) dx \quad \text{Eqn. 4-29}$$

$$N = -\frac{1}{2} \rho_{water} \int_{-L/2}^{L/2} T(x) C_d^{2D}(x) x |v_r + xr| (v_r + xr_r) dx \quad \text{Eqn. 4-30}$$

$$Z = -\frac{1}{2} \rho_{water} \int_{-L/2}^{L/2} T(x) C_d^{2D}(x) |w_r + xr| (v_r + xr_r) dx \quad \text{Eqn. 4-31}$$

$$M = -\frac{1}{2} \rho_{water} \int_{-L/2}^{L/2} T(x) C_d^{2D}(x) x |w_r + xr| (v_r + xr_r) dx \quad \text{Eqn. 4-32}$$

Where $T(x)$ is the draft (in our case the diameter of the AUV), v_r is the relative linear velocity in the Y_B direction, w_r is the relative linear velocity in the Z_B direction, r_r is the relative angular velocity about the Z_B axis, and $C_d^{2D}(x)$ is a cross flow drag coefficient that can be estimated using Hoerner's curve, Figure 8.

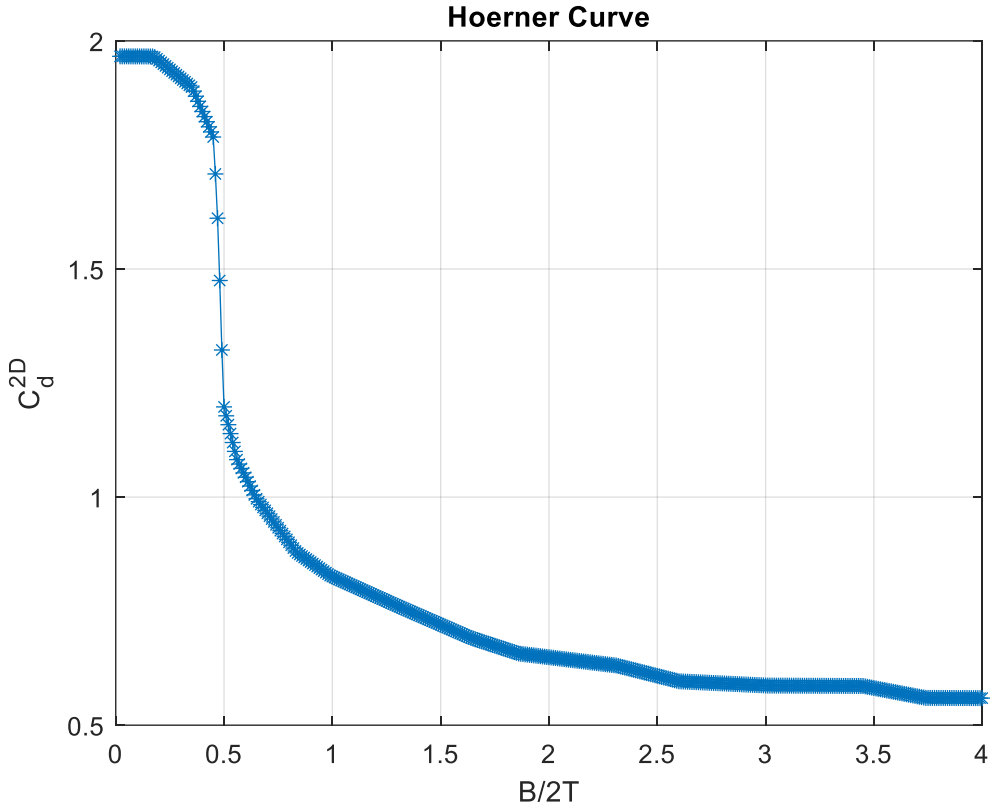


Figure 8: Hoerner Curve

4.6.4 Rudder Sway Force/Moment

The rudder is located on the rear side of the AUV and is used to control the rotation of the vehicle about the Z_B axis. Since the rudder at rest is nominally aligned with the $X_B Z_B$ plane it exerts a lift force perpendicular to that plane, in the Y_B direction

$$\tau_{input}(2) = Y_{rudder} = -\frac{1}{2} \rho_{water} V_{rh}^2 A_r C_{Lr} \delta_r \quad \text{Eqn. 4-33}$$

Where V_{rh} is the relative speed in the horizontal plane ($V_{rh} = \sqrt{v_{rel}^B(1)^2 + v_{rel}^B(2)^2}$), A_r is the rudder area, C_{Lr} is the rudder lift coefficient, and δ_r is the rudder angle [3].

Using the rudder, X_B position in the body frame, x_{rudder} , a moment is produced acting about the Z_B axis:

$$\tau_{input}(6) = x_{rudder} \cdot Y_{rudder} \quad \text{Eqn. 4-34}$$

4.6.5 Stern Plane Heave Force/Moment

The stern plane is located on the rear side of the AUV and is used to control the rotation of the vehicle about the Y_B axis. Since the stern at rest is nominally aligned with the $X_B Y_B$ plane it exerts a lift force perpendicular to that plane, in the Z_B direction

$$\tau_{input}(3) = Z_{stern} = -\frac{1}{2} \rho_{water} V_{rv}^2 A_s C_{L_s} \delta_s \quad \text{Eqn. 4-35}$$

Where V_{rv} is the relative speed in the vertical plane ($V_{rv} = \sqrt{v_{rel}^B(1)^2 + v_{rel}^B(3)^2}$), A_s is the stern plane area, C_{L_s} is the stern lift coefficient, and δ_s is the stern plane angle [3].

Using the stern, X_B position in the body frame, x_{stern} , a moment is produced acting about the Y_B axis:

$$\tau_{input}(5) = x_{stern} \cdot Z_{stern} \quad \text{Eqn. 4-36}$$

4.7 Plant Model in Terms of Absolute Velocity

To represent the plant model in absolute velocity, velocity in the NED frame, first consider Eqn. 4-1 which is a function of both the general velocity, v_G^B , and the relative velocity, v_{rel}^B , in the body frame. In order to utilize the relationships between the body and NED frame derived in Section 3.2.2, we must first specify Eqn. 4-1 in terms of just v_{rel}^B . This requires modification of the rigid body mass and Coriolis-centripetal terms.

Since the rigid body Coriolis-centripetal matrix given by Eqn. 4-9 is independent of the linear velocity, and given the irrotational current assumption made in Section 4.1, $C_{RB}(v_G^B) = C_{RB}(v_{rel}^B)$

We can show that

$$M_{RB}^{CO} \dot{v}_c^B + C_{RB}^{CO}(v_{rel}^B) v_c^B = 0 \quad \text{Eqn. 4-37}$$

By using Eqn. 4-5 and Eqn. 4-9 to expand the expression out

$$\begin{aligned} & \begin{bmatrix} mI_{3x3} & -mS(r_G^B) \\ mS(r_G^B) & I_G - mS^2(r_G^B) \end{bmatrix} \begin{bmatrix} -S(\omega_{B/N}^B) v_c^B \\ 0 \end{bmatrix} \\ & + \begin{bmatrix} mS(\omega_{B/N}^B) & -mS(\omega_{B/N}^B) S(r_G^B) \\ mS(r_G^B) S(\omega_{B/N}^B) & mS(r_G^B) S(\omega_{B/N}^B) S^T(r_G^B) - S(I_G \omega_{B/N}^B) \end{bmatrix} \begin{bmatrix} v_c^B \\ 0 \end{bmatrix} = 0 \end{aligned} \quad \text{Eqn. 4-38}$$

From Eqn. 4-37, it follows that

$$\begin{aligned} M_{RB} \dot{v}_G^B + C_{RB}(v_G^B) v_G^B &= M_{RB} [\dot{v}_{rel}^B + v_c^B] + C_{RB}(v_{rel}^B) [v_{rel}^B + v_c^B] \\ &= M_{RB} \dot{v}_{rel}^B + C_{RB}(v_{rel}^B) v_{rel}^B \end{aligned} \quad \text{Eqn. 4-39}$$

Therefore Eqn. 4-1 can be written strictly in terms of the relative velocity in the body frame

$$\begin{aligned} & M_{RB} \dot{v}_{rel}^B + C_{RB}(v_{rel}^B) v_{rel}^B + M_A \dot{v}_{rel}^B + C_A(v_{rel}^B) v_{rel}^B \\ & + D(v_{rel}^B) v_{rel}^B + g(\eta) \\ & = \tau_{Input} + \tau_{Current} + \tau_{DragLift} + \tau_{CrossFlowDrag} \end{aligned} \quad \text{Eqn. 4-40}$$

Note that

$$\dot{v}_G^B = \dot{v}_c^B + \dot{v}_{rel}^B = -S(\omega_{B/N}^B)v_c^B + \dot{v}_{rel}^B \quad \text{Eqn. 4-41}$$

And that the velocity in NED frame can be derived from the velocity in the body frame through the relationships given by Eqn. 3-2 and Eqn. 3-10

$$v_G^N = \begin{bmatrix} R_B^N & 0_{3x3} \\ 0_{3x3} & (T_N^B)^{-1} \end{bmatrix} v_G^B \quad \text{Eqn. 4-42}$$

5 Emulation Setup

To emulate the nonlinear continuous time plant in the discrete time we setup a MATLAB script that will call ODE45 within a for loop solving the nonlinear state equations given iteration varying inputs.

The system can best be described by Figure 9.

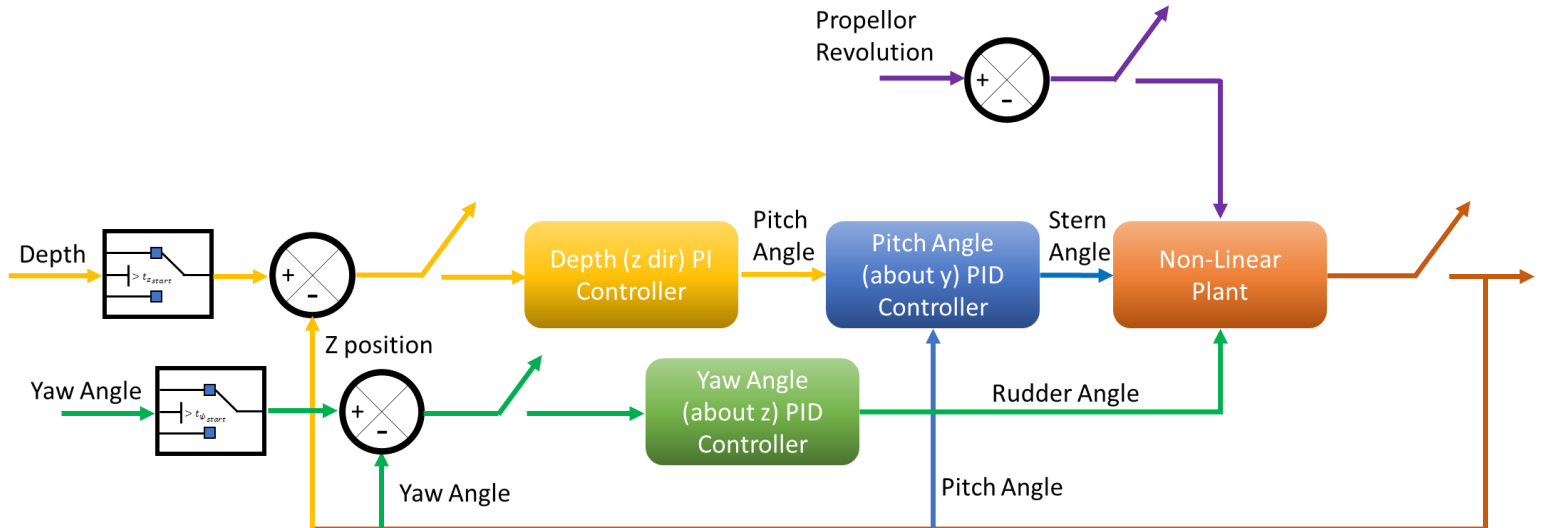


Figure 9: System Block Diagram

There are 3 continuous reference inputs to the system: a propeller revolution profile, a depth profile, and a yaw angle profile. There is a delayed on the start of the depth and yaw angle references to ensure completion of other profiles. First the propeller ramps up to max speed; shortly after it saturates, the depth reference input kicks on and the vehicle dives to a depth of 30 meters (represented by a ramp input). Lastly, once the vehicle is at depth, the yaw angle trajectory engages and the AUV tracks heading the profile. We investigated 3 different yaw angle trajectories. Figure 10 is a visual representation of the reference inputs.

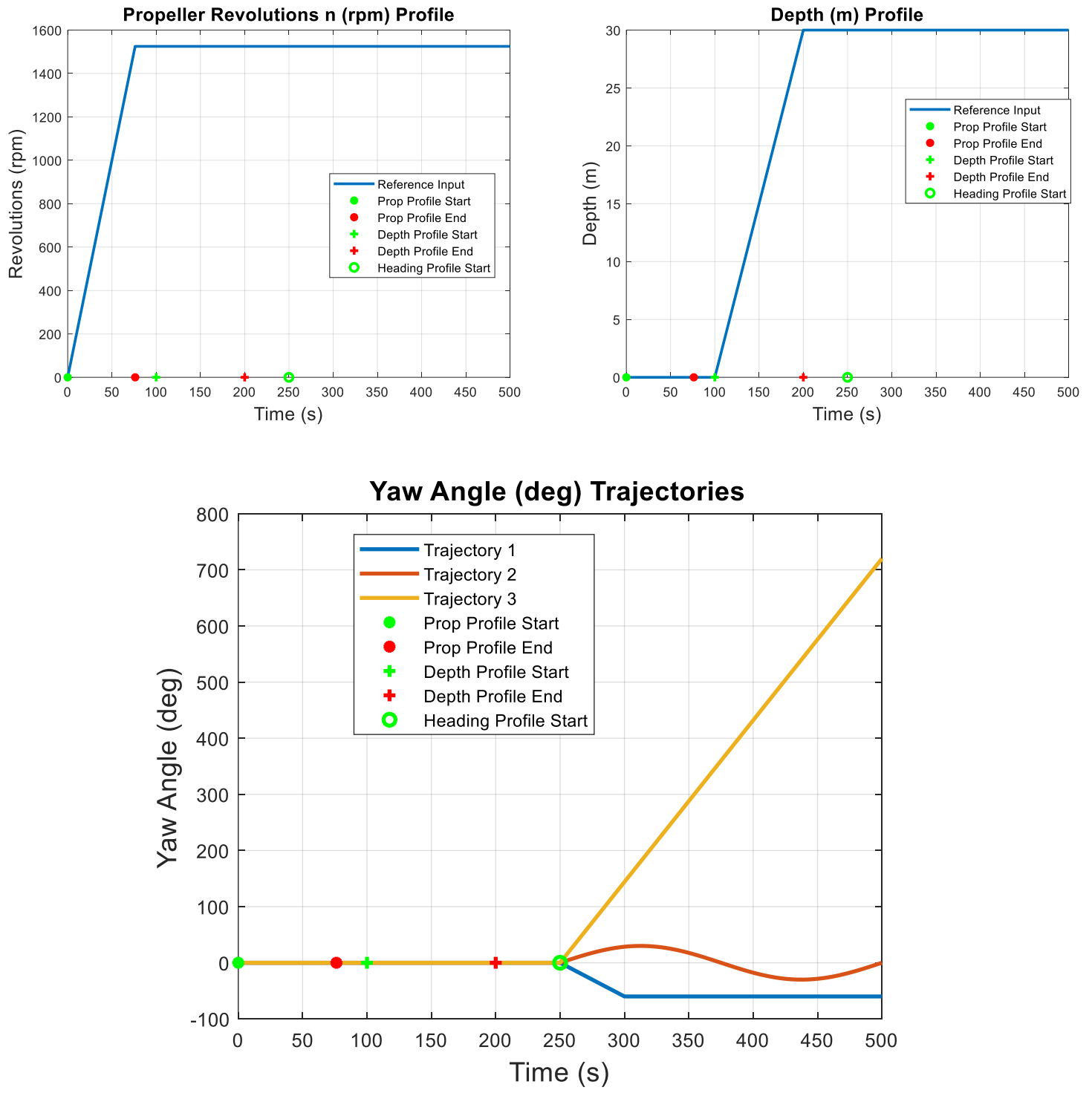


Figure 10: Reference Inputs/Trajectories

Samplers in Figure 9 indicate transitions from continuous time to discrete time. Continuous time reference signals are sampled at a specified sampling rate to provide inputs into either the controller and subsequently the plant model or directly to the plant model. The plant model is a continuous time model, the states are solved for using ODE45 making the output of the system inherently discrete. The MATLAB ODE solver subsamples the sampling time to arrive at a solution to the state space equations; from the entire output data set we only utilize the end point (states associated with the specified sampling time). The state space model will be discussed in detail in section 5.1. Specific states are feedback to specific controllers. A description of each of the controllers is presented in section 5.3. The three controllable inputs: propellor revolution speed, rudder angle, and stern plane angle are fed into the nonlinear model. Within the plant model is a relationship between those three inputs and the 6x1 input matrix of three forces (in each axis direction) and three moments (about each axis) that are fed into the equations of motion; section 5.2 will provide more detail about the inputs.

5.1 State Space Representation

The plant model is represented in the NED reference frame, all subsequent angles and velocities are computed in that frame.

The 6 DOF plant model allows for 12 states, the 6 velocities (3 linear and 3 angular) and 6 positions (3 cartesian coordinates and 3 angles)

$$\dot{v}_{rel}^B = \begin{bmatrix} \dot{u} \\ \dot{v} \\ \dot{w} \\ \dot{p} \\ \dot{q} \\ \dot{r} \end{bmatrix} = [-(M)^{-1}(C + D(v_{rel}^B))] \begin{bmatrix} u \\ v \\ w \\ p \\ q \\ r \end{bmatrix} + (M)^{-1} \begin{bmatrix} \tau_{Prop} \\ Y_{rudder} \\ Z_{stern} \\ 0 \\ x_{stern} \cdot Z_{stern} \\ x_{rudder} \cdot Y_{rudder} \end{bmatrix} + (M)^{-1} (\tau_{DragLift} + \tau_{CrossFlowDrag} - g(\eta^N)) + (M)^{-1} \tau_{Current} \quad \text{Eqn. 5-1}$$

where

$$M = (M_{RB} + M_A), \quad C = (C_A(v_{rel}^B) + C_{RB}(v_{rel}^B))$$

Recalling the relationships Eqn. 4-41 and Eqn. 4-42, the overall state space equation is given by

$$\begin{bmatrix} \dot{v}_G^B \\ \dot{\eta}^N \end{bmatrix} = \begin{bmatrix} -S(\omega_{B/N}^B)v_c^B \\ 0_{6x1} \end{bmatrix} + \begin{bmatrix} \dot{v}_{rel}^B \\ 0_{6x1} \end{bmatrix} + \begin{bmatrix} R_B^N & 0_{6x6} \\ 0_{3x3} & (T_N^B)^{-1} \end{bmatrix} \begin{bmatrix} v_G^B \\ \eta^N \end{bmatrix} \quad \text{Eqn. 5-2}$$

5.2 Inputs Discussion

A AUV typically has 3 controllable inputs: propellor revolution speed, rudder angle, and stern plane angle.

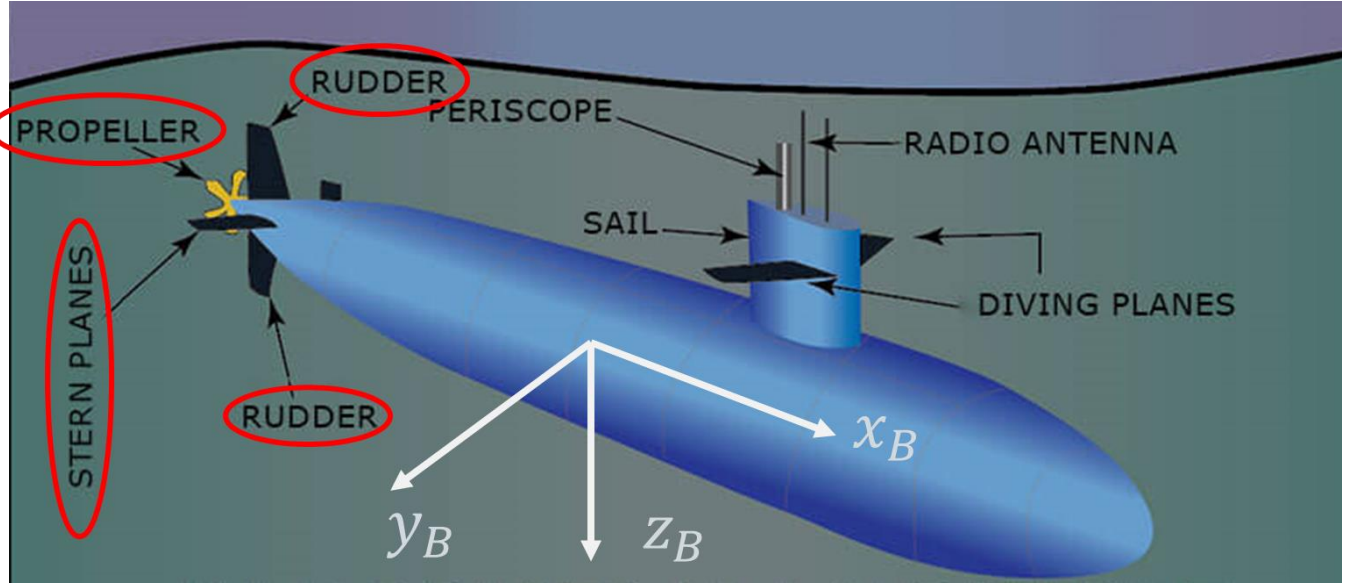


Figure 11: Controllable inputs

The plant model has 12 states, 3 controllable inputs which can be related to the 6 inputs (forces in the direction of, and moments about each body axis). At most the rank of the controllability matrix can be 6, therefore the system is not fully controllable.

Through propeller revolution speed, it is possible to indirectly affect the velocity states. A relationship to the position of the vehicle can be derived as well assuming the initial position is known.

The remaining question is, how do these controllable inputs to the hardware relate to the inputs of the plant model? The propeller has contributions to the force in the x_b direction. We neglect the contribution of the rotation of the propeller on the moment about the x_b axis due to the small enough size of the propeller.

The rudder position has contributions to the force in the x_b direction, and the force in the y_b direction (through the lift force derived in section 4.6.4). The force acting in the y_b direction exerts a moment about the z_b axis.

The stern plane angle has contributions to the force in the x_b direction, and the force in the z_b direction (through the lift force derived in section 4.6.5). The force acting in the z_b direction exerts a moment about the y_b axis.

The relationship between the three controllable inputs and the force in the x_b direction involves a complicated motor model which we did not derive for our project. Simplifying the model presented in reference [1], we assume the relationship to be

$$\tau_{Input}(1) = \tau_{Prop} = c_1 n_{rev}^2 + c_2 n_{rev} V_{lin} + c_r \delta_r^2 V_{rh}^2 + c_s \delta_s^2 V_{rv}^2$$

where

$$V_{lin} = \sqrt{v_G^B(1)^2 + v_G^B(2)^2 + v_G^B(3)^2}$$

$$V_{rh} = \sqrt{v_{rel}^B(1)^2 + v_{rel}^B(2)^2}$$
Eqn. 5-3

$$V_{rv} = \sqrt{v_{rel}^B(1)^2 + v_{rel}^B(3)^2}$$

Where c_1, c_2, c_r, c_s are constants we identified from parameters in [1] associated with the motor model, n_{rev} is the propellor revolution, δ_r is the rudder angle, δ_s is the stern plane angle, V_{lin} is the speed of the vehicle, V_{rh} is the relative horizontal speed, and V_{rv} is the relative vertical speed.

5.3 PID controllers

The system incorporates 3 discrete time PID controllers. See Figure 9 for how they are incorporated into the control loop.

1. Depth controller – computes error from depth reference input and z position feedback (model output), Outputs a desired pitch angle.

$$\theta_d = K_{p_z}(z - z_{ref}) + K_{I_z} \cdot T_s \sum_{j=0}^k (z(j) - z_{ref}(j)) \quad \text{Eqn. 5-4}$$

2. Pitch angle controller – computes error from desired pitch angle (output of depth controller) and pitch angle feedback (model output). Outputs a desired stern plane angle.

$$-\delta_s = K_{p_\theta}(\theta - \theta_d) + K_{D_\theta}q + K_{I_\theta} \cdot T_s \sum_{j=0}^k (\theta(j) - \theta_d(j)) \quad \text{Eqn. 5-5}$$

3. Yaw angle controller- computes error from yaw angle reference input and yaw angle feedback (model output), Outputs a desired rudder angle.

$$-\delta_r = K_{p_\psi}(\psi - \psi_{ref}) + K_{D_\psi}r + K_{I_\psi} \cdot T_s \sum_{j=0}^k (\psi(j) - \psi_d(j)) \quad \text{Eqn. 5-6}$$

The controller coefficients were taken from reference [1]. The author sets up a simulation on an external marine craft modeling software package to identify coefficients for the operating conditions of the system. It looks like the software package is linearizing the system around defined equilibrium conditions and testing against realistic ocean currents to identify PID gains.

5.4 MIMO to SISO Discussion

As noted in Figure 9 and Figure 10, there is a delay in introduction of the 3 reference inputs; only upon arrival to a new equilibrium state does a new reference command begin. First the propellers are brought to speed, then the vehicle begins its descent to its desired depth, once at depth a heading profile is introduced. This is done to reduce the cross effects of the three controllable inputs on the system's ability to track the three different references. Given our plant model, the off-diagonal terms of the mass and Coriolis matrices could adversely affect the controllers' capabilities to track the reference input should they be presented all at once. By introducing each

input one at a time and allowing the system to stabilize at new intermediate equilibrium points we minimize the magnitude of those off diagonal terms and reduce interference of an input on untargeted states. This allows for the utilization of SISO PID controllers to correct for errors in the actual state trajectory relative to the desired trajectories and subsequently produce the appropriate force/moment commands to the plant without having to consider MIMO control theory.

6 Results

All our results assessments were performed qualitatively. Our performance metrics for the control loop are:

1. Is the system stable?
2. Can it track different trajectories? To assess this, we looked at 3 different heading angle trajectories. The various trajectories are given by Figure 10
3. Is the system robust against disturbances? To assess this, we considered 2 ocean current speeds and 2 sideslip angles (β as defined in Section 3.2.3)

Ocean current speed:

1. Realistic: .5 m/s, the average current velocity at the ocean surface
2. Worst case: 1.8 m/s, the average current velocity of the gulf stream

Ocean current sideslip angles

1. Fixed at a constant value of 33 degrees; the angle orthogonal to the vessel at the final yaw position of trajectory 1.
2. A time varying worst case where the angle always remains orthogonal to the vessel

The following sections will discuss how we meet these metrics

6.1 Simulation Parameters

Parameter	Value
Sampling rate (for all but sampling time analysis section)	0.05s
Number of Samples	10000
Propeller revolution input	1525 rpm
Depth input	30 m
Start of Depth Input	100 seconds
Trajectory 1	Ramp to constant yaw angle of -60 deg
Trajectory 2	Yaw angle sine wave path
Trajectory 3	Constant ramping yaw angle from 0 - 2π
Start of Heading Input	250 seconds
Ocean current realistic speed	0.5 m/s
Ocean current worst-case speed	1.8 m/s

Fixed current sideslip angle	33 deg
Uniform AUV density	1026 kg/m ³
Non-uniform AUV density	[800 (for front 90 %) 1026 (for rear)] kg/m ³
Length of AUV	1.6 m
Diameter of AUV	.19 m
K_{p_z}	.1
K_{I_z}	.001
K_{p_θ}	2
K_{D_θ}	3
K_{I_θ}	.1
K_{p_ψ}	7.5
K_{D_ψ}	15
K_{I_ψ}	.75

6.2 Sampling Time Analysis

Identifying an appropriate sampling time involved employing a guess and check method. Two criteria needed to be meet when selecting a sampling time:

1. The sampling time must be small enough to keep the system stable.
2. The sampling time must be large enough to keep computation burden low and subsequently run time reasonable.

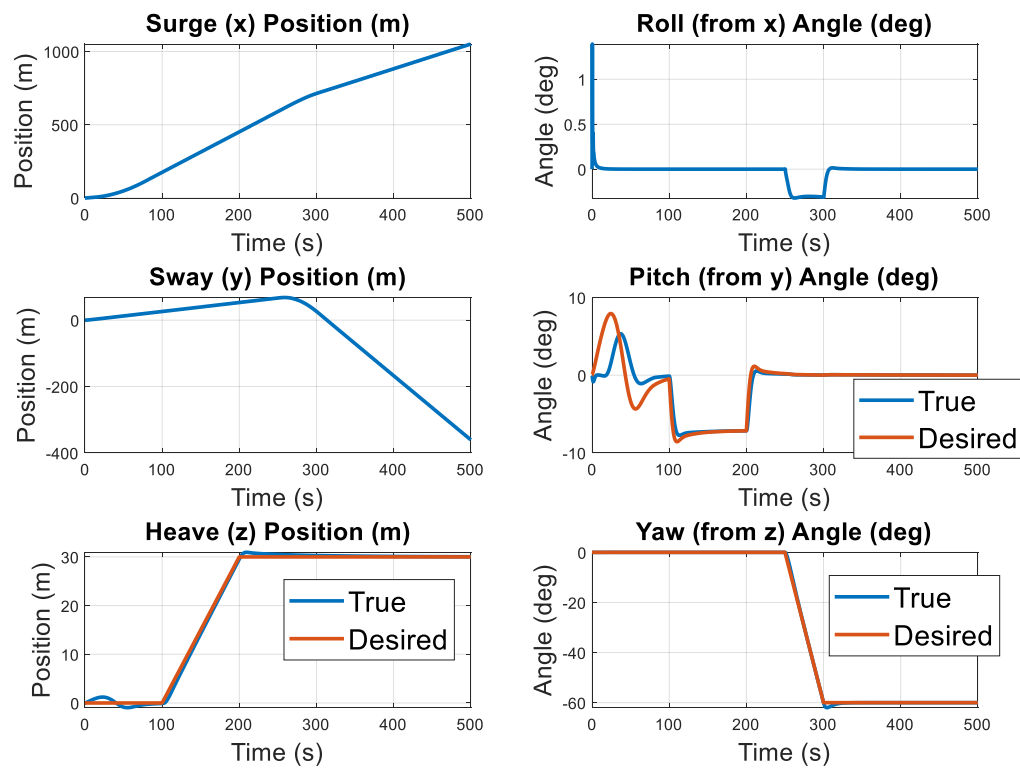
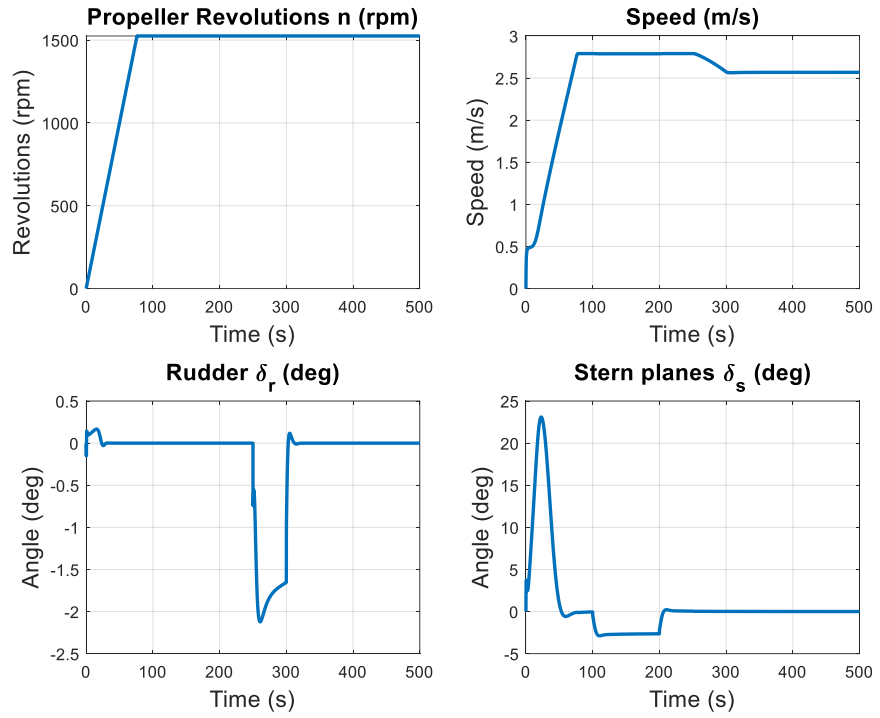
As a baseline we used yaw trajectory 1 (Figure 10), realistic ocean current speed, and a fixed sideslip angle.

The simulation results (system inputs, position state, and velocity states) for 2 sampling times are presented in the figures below.

Figure 12 exercises a .05 second sampling time, this sampling time is the one selected to be our ideal sampling time. All subsequent simulations were performed using this sampling time.

Figure 13 exercises a .15 second sampling time; the onset of instability occurs at this sampling time. This is apparent by the rapid oscillations observed in the roll and yaw rates.

In addition, a sampling time of .01 seconds was assessed. There was an unnoticeable difference in the results at the cost of an additional few minutes of run time. Given the burden placed on a desktop, should one later wish to employ this control scheme on the REMUS 100 hardware, it may be an unrealistic expectation given the reduced specs of any processor/memory on board. At a rate of .05 seconds, for the cases tested, the control loop produces adequate results.



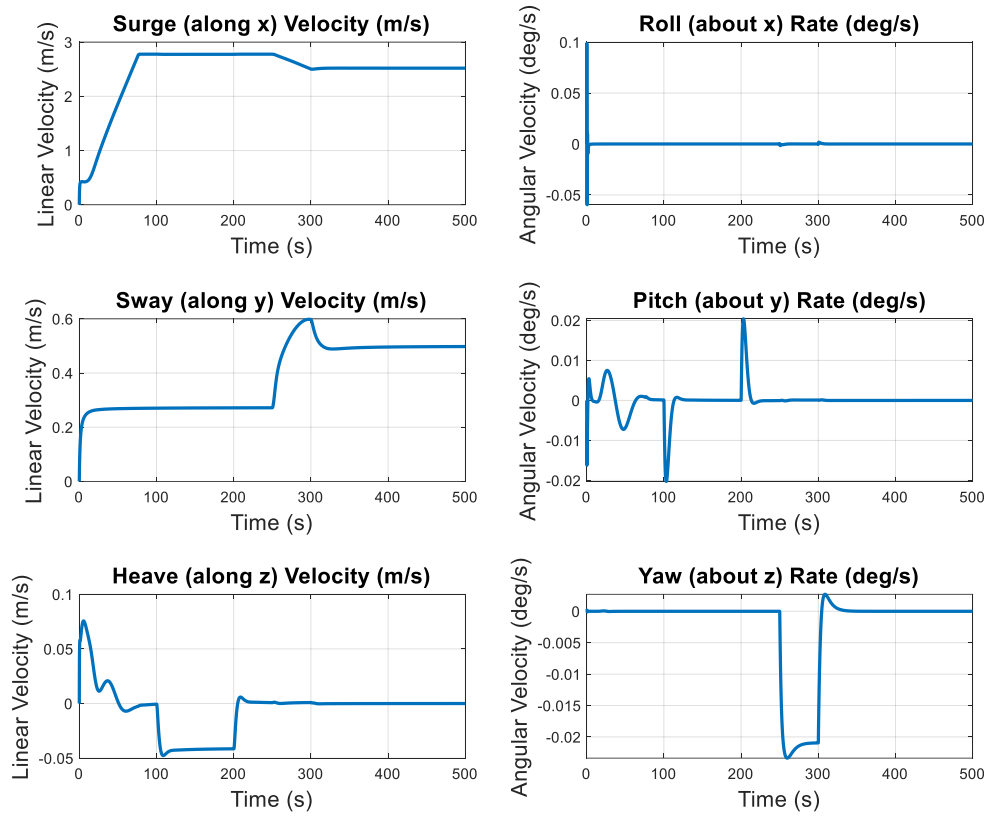
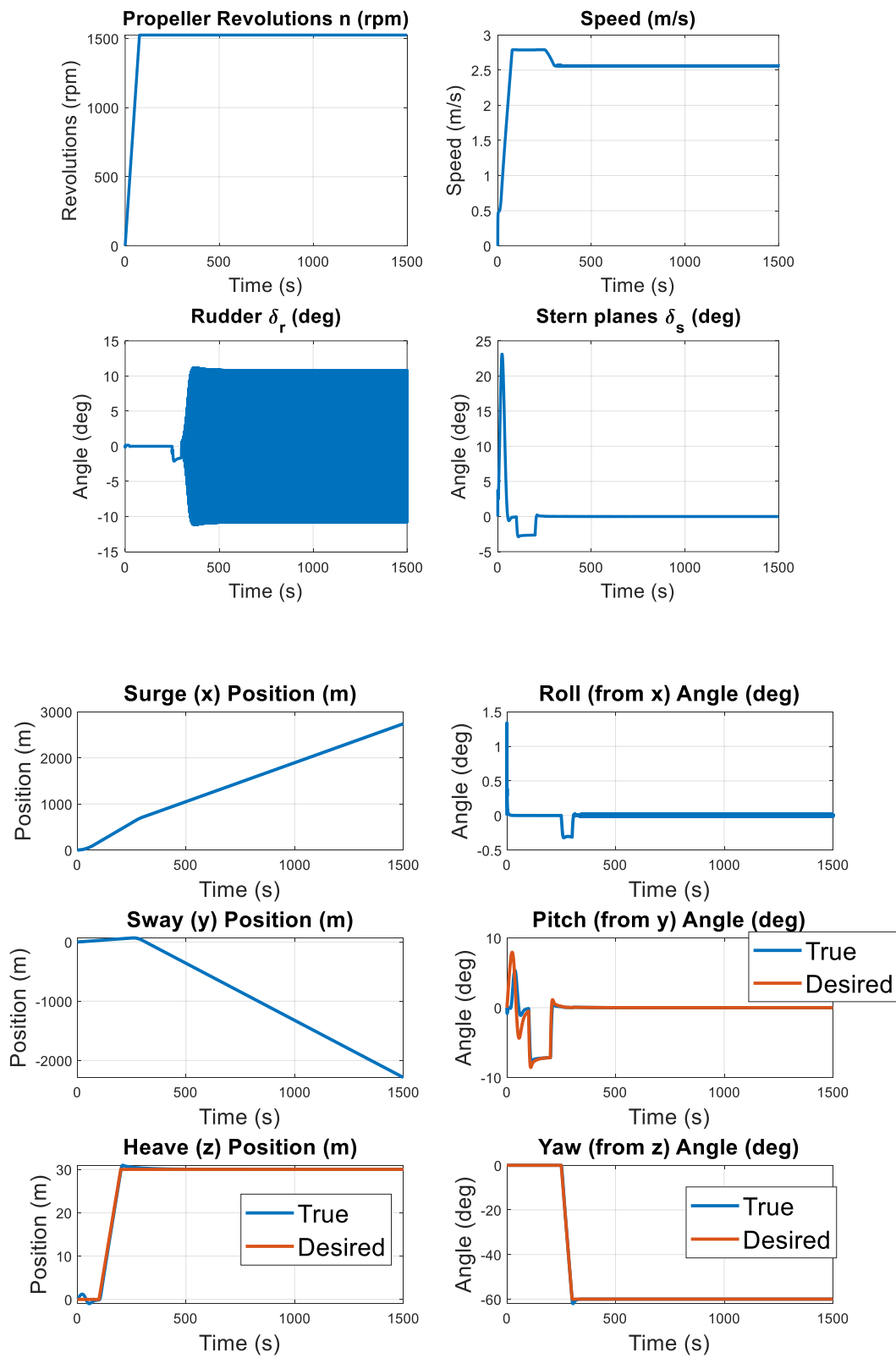


Figure 12: Sampling time analysis. Sampling time = .05 seconds (20 Hz), yaw trajectory 1, .5 m/sec current speed, fixed sideslip angle



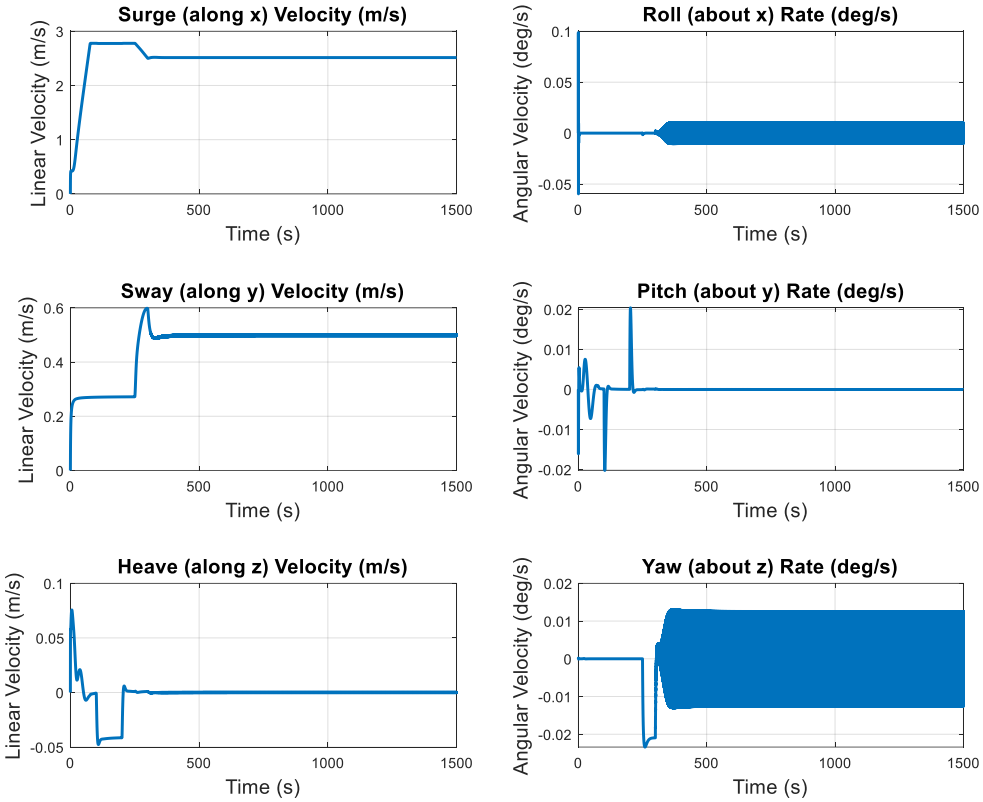
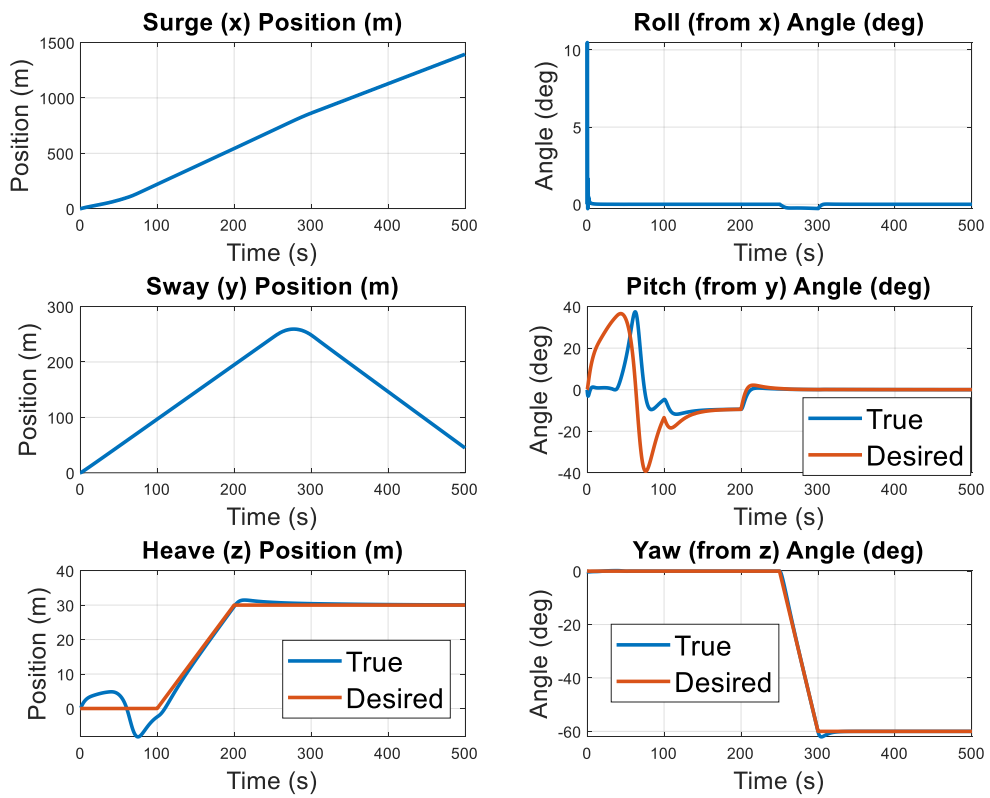
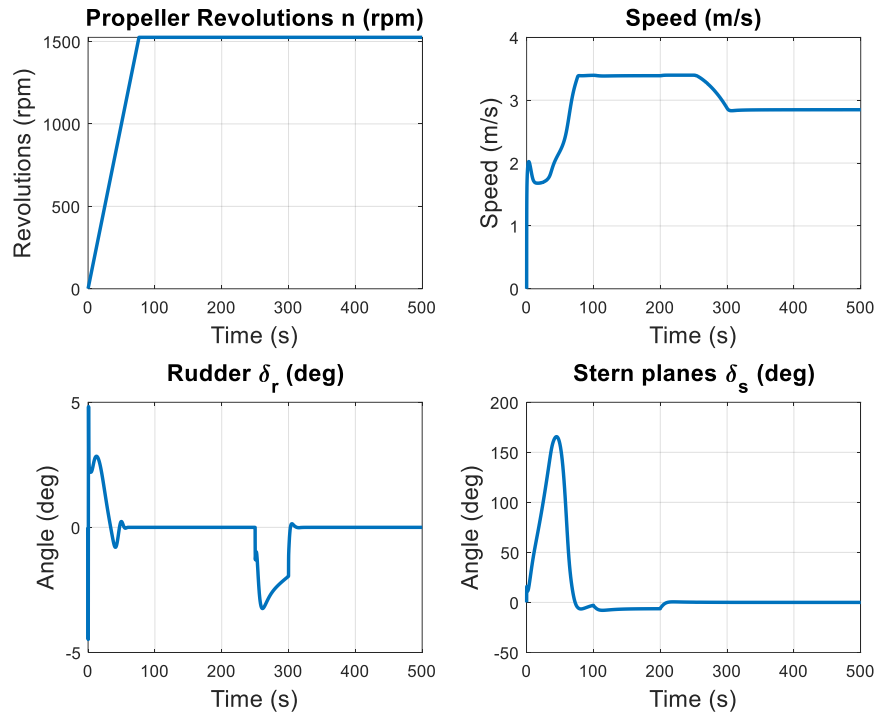


Figure 13: Sampling time analysis. Sampling time = .15 seconds (6.67 Hz), yaw trajectory 1, .5 m/sec current speed, fixed sideslip angle

6.3 Trajectory 1, Fast Current

To satisfy performance metric 2 and 3, we looked at 3 different trajectories under variations of disturbances. The first trajectory is a simple ramp up to a constant yaw angle and hold. This trajectory was simulated using the low current speed (Figure 12) and fast current speed (Figure 14). Both simulations ran with the fixed β angle; the effect of the time varying, worst case β was found to be negligible as fixed β angle applied the orthogonal current condition for the majority of the profile (the final held position).



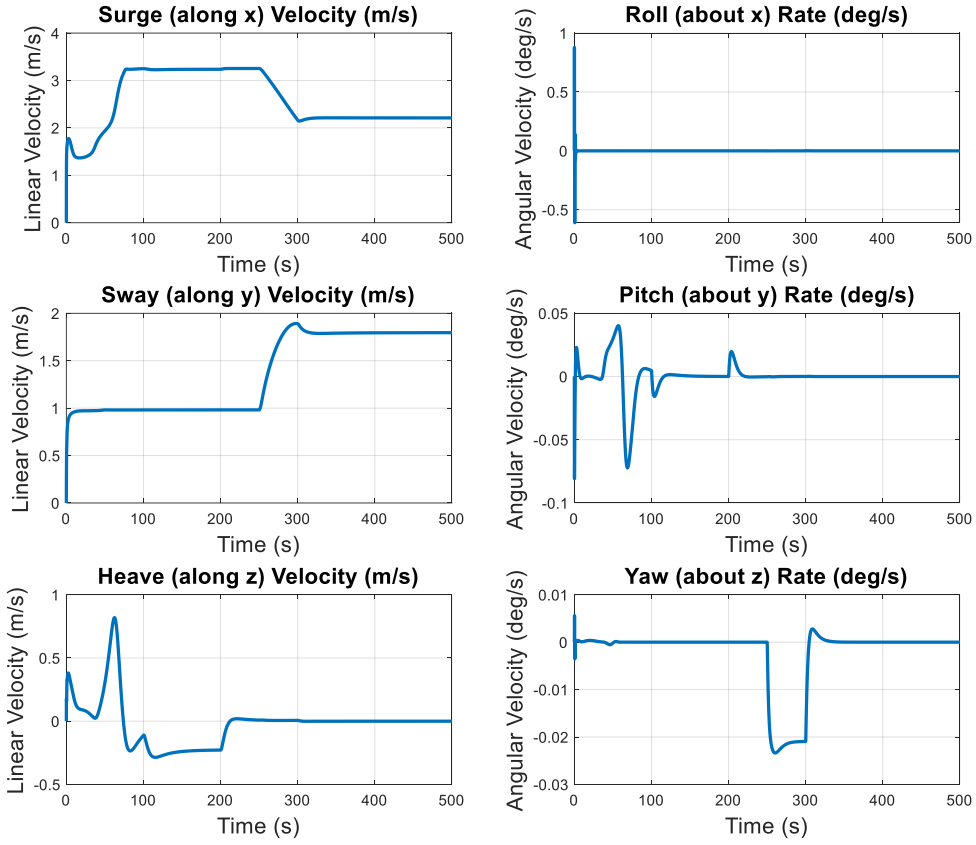


Figure 14: Trajectory I Tracking. Sampling time = .05 seconds (20 Hz), yaw trajectory 1, 1.5 m/sec current speed, fixed sideslip angle

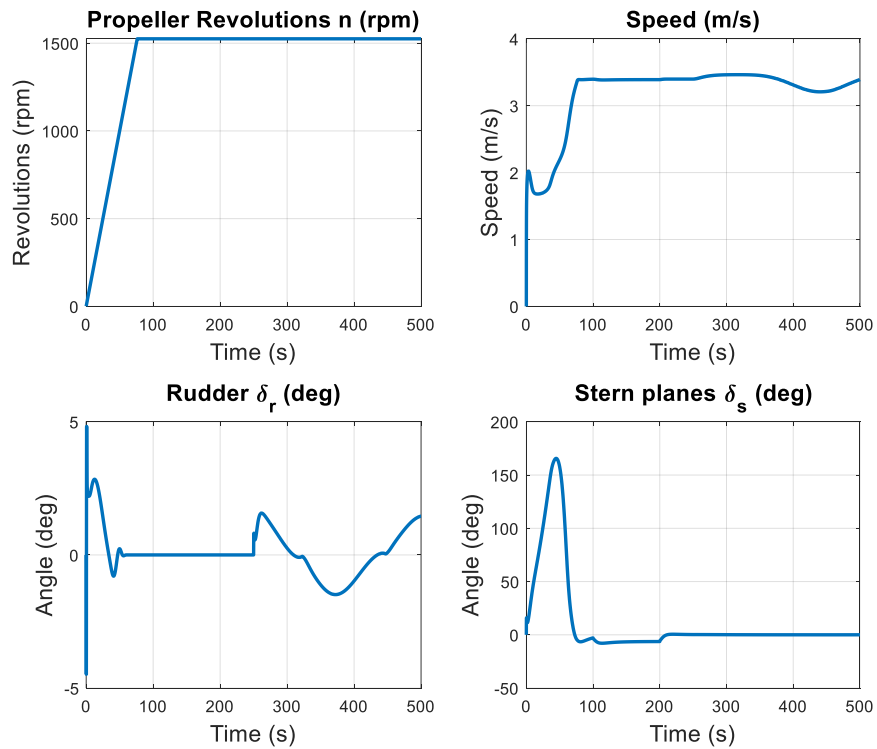
When comparing the states between the two different disturbance cases, the first notable observation is the differences in the sway positions of the vehicle. When being perturbed orthogonally by horizontal ocean currents, the vehicle is being pushed in this direction resulting in the differences seen between the two. This motion in sway is observable in the sway velocity state as well.

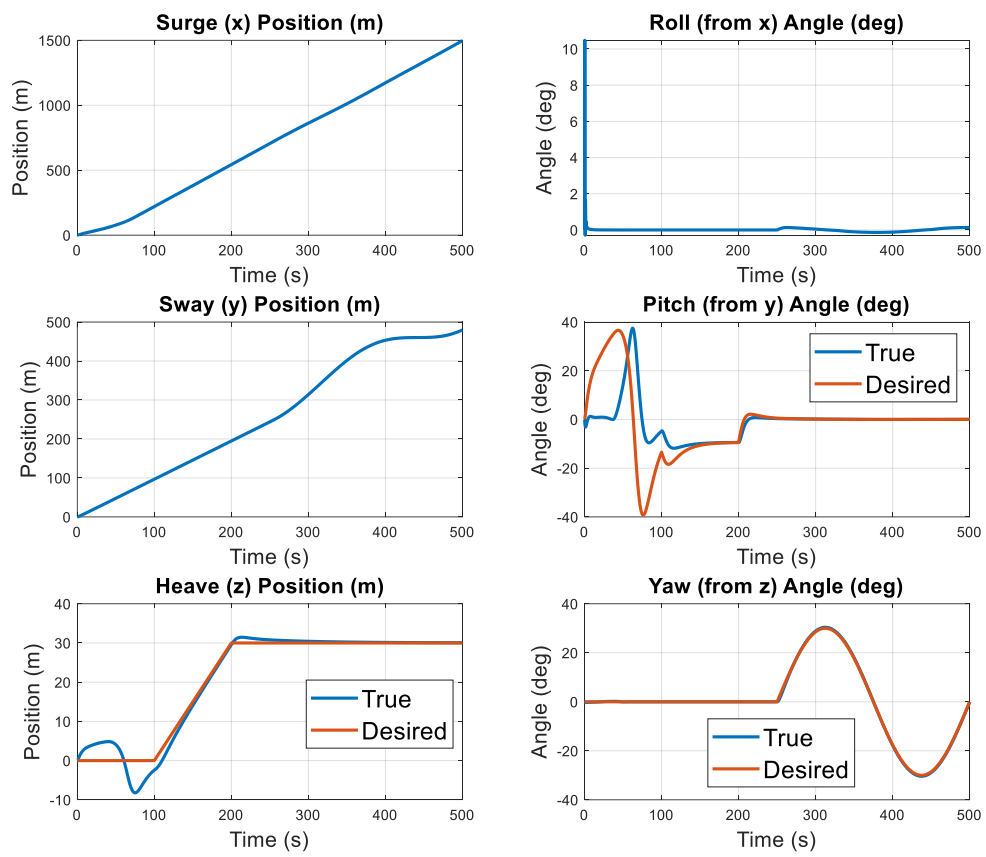
Another interesting observation is that the increased current speed has an adverse effect on the pitch angle. As the vehicle tries to dive down, it is met with an increased resistance acting in the horizontal plane, the plane that it is trying to break through to move deeper. As a result, the controller is forced to output larger stern plane angles to achieve the larger forces to propel the vehicle and moments required to turn it downwards. The desired pitch angles are greater, and the controller has an increased difficulty tracking them under the fast current condition up until we reach an equilibrium depth of 30 m. As an effect of the increased effort in pitch, the heave position tracking also suffers.

The controller can track the yaw angle with a high level of accuracy, although we do observe a larger rudder angle needed to compensate for the increased current speed pushing against it in the direction orthogonal to the final yaw angle.

6.4 Trajectory 2, Fast Current

To continue our assessment of performance metric 2, we consider a different heading angle profile, trajectory 2 given by Figure 10. This trajectory moves the yaw angle in a sine wave like profile. To satisfy performance metric 3 we look at the effect of the fast current when trying to track the new heading angle. Figure 15 below shows the results from this simulation using the fixed β angle. We attempted the simulation using the worst case, time varying β angle, but the controller failed to track the reference inputs under this condition. It is possible that with the constantly changing yaw angle the yaw controller was unable to adjust and compensate quickly enough. Given that this is an unrealistic condition created merely to assess the worst case, we noted this failure and proceeded with just the current speed increase.





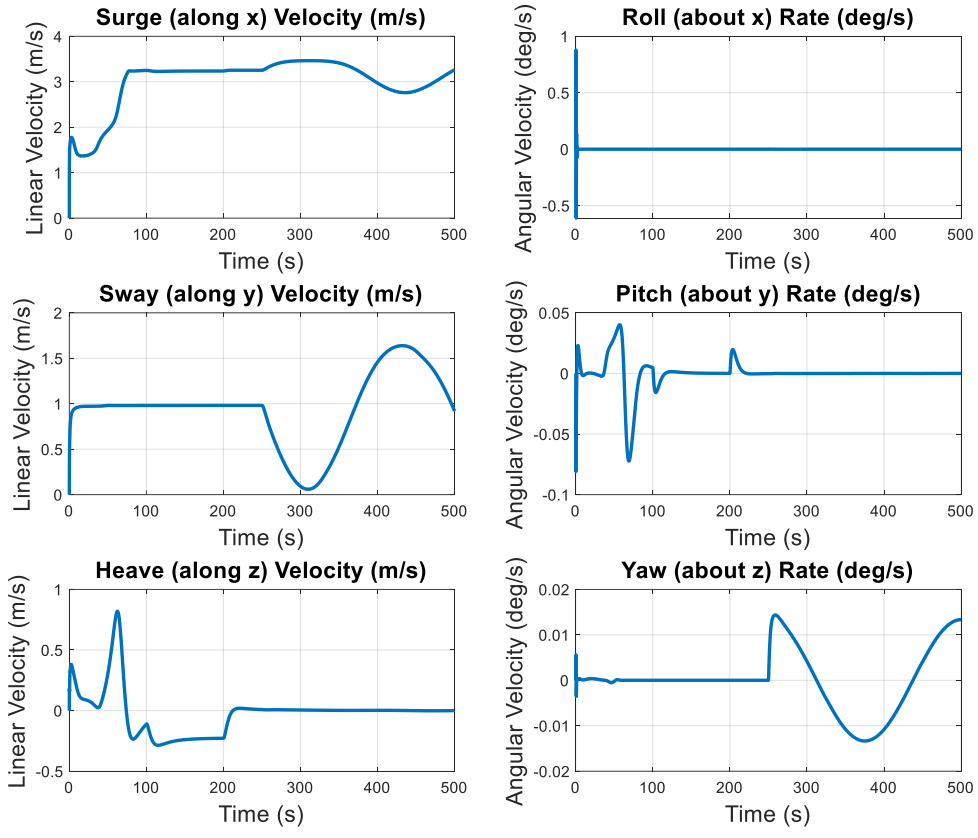


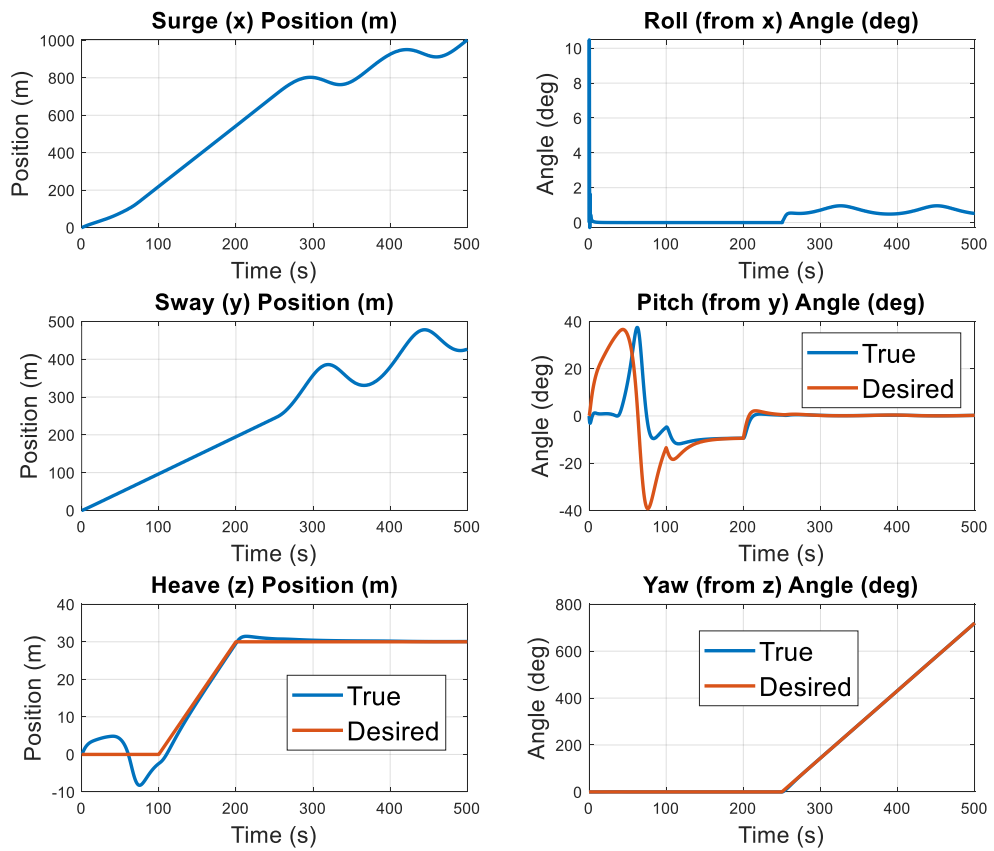
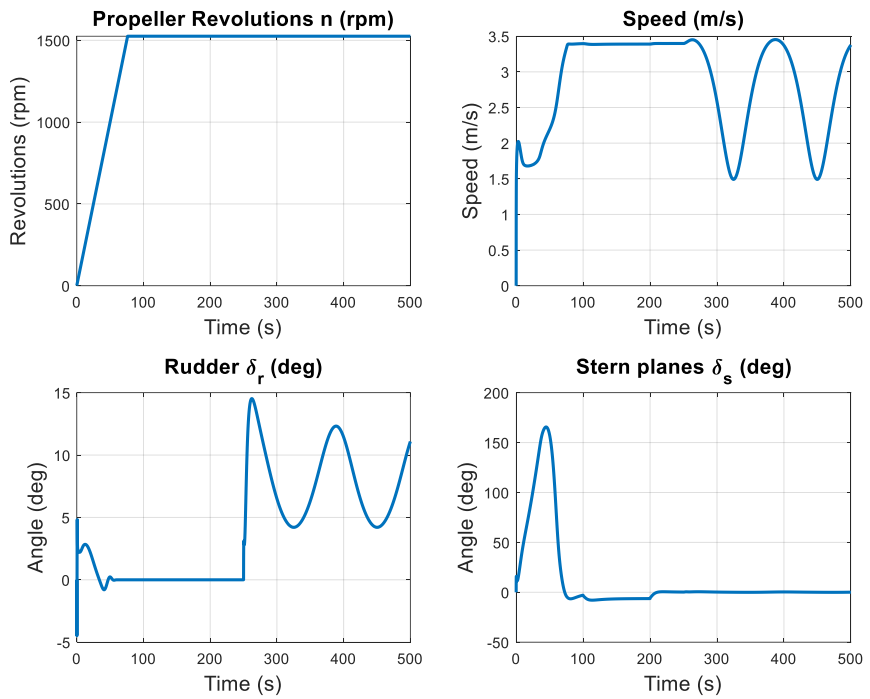
Figure 15: Trajectory 2 Tracking. Sampling time = .05 seconds (20 Hz), yaw trajectory 2, 1.5 m/sec current speed, fixed sideslip angle

The same trends in sway position/velocity, pitch angle/rate, and heave position/velocity observed with trajectory 1 and discussed in section 6.3, appear here as well. This is expected because the only variation between the two cases is the yaw angle trajectory, which does not influence the vehicle diving.

The only result of notable interest now is how well yaw controller follows the new trajectory. Qualitatively speaking, it does an excellent job at tracking the sine wave profile as the desired and true curves nearly overlap one another. The rudder angle changes accordingly, producing force/moment output necessary to follow the new heading path.

6.5 Trajectory 3, Fast Current

Lastly, to conclude our assessment of performance metric 2, we considered trajectory 3 given by Figure 10. Trajectory 3 is a constantly ramping yaw angle cycling from 0 to 2π , intended to spin the vehicle around the z_B axis. Like the previous simulations we assessed this trajectory against the fast current speed using a constant β angle. Similar to trajectory 2, trajectory 3 failed to track under the worst case, time varying β angle condition. Figure 16 presents the results of the trajectory 3 simulation.



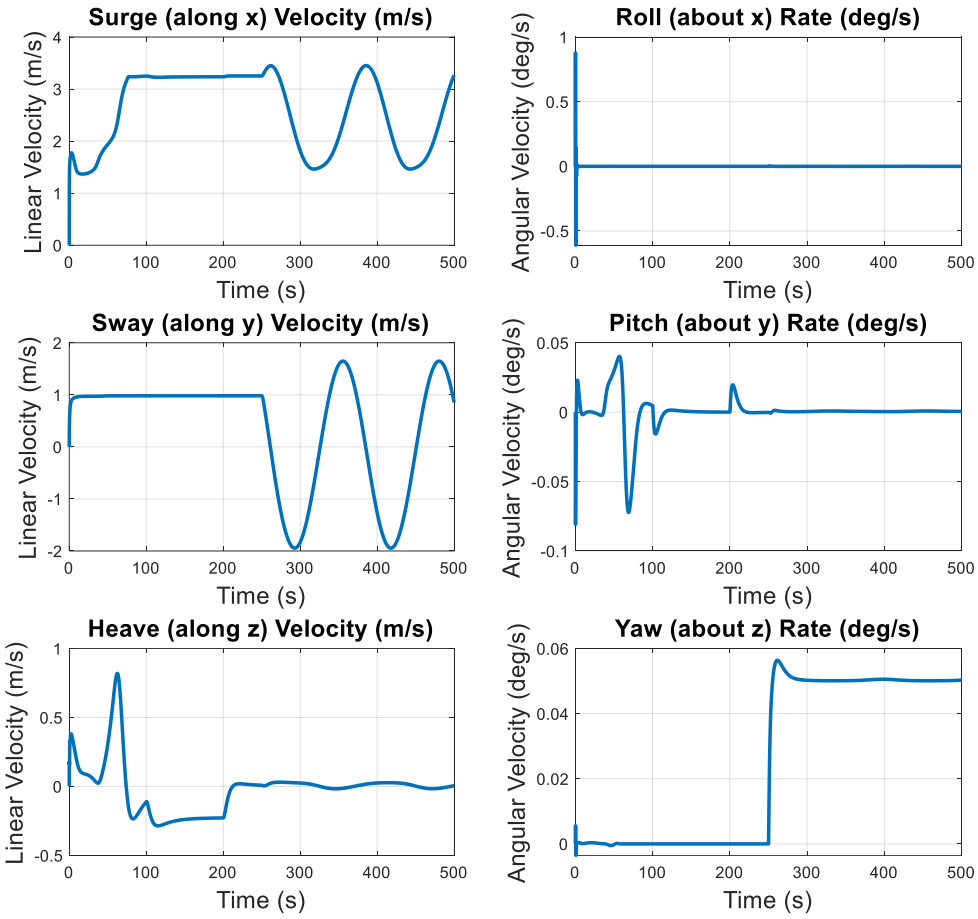


Figure 16: Trajectory 3 Tracking. Sampling time = .05 seconds (20 Hz), yaw trajectory 3, 1.5 m/sec current speed, fixed sideslip angle

Again, we observe similar effects of the fast current on sway position/velocity, pitch angle/rate, and heave position/velocity noted before. There are notable differences between the plots of these states across the 3 different trajectories. However, the reasoning behind this is unclear to us currently and requires further investigation.

We note that the yaw angle controller is able to track the new trajectory without any issues, the qualitative performance is excellent.

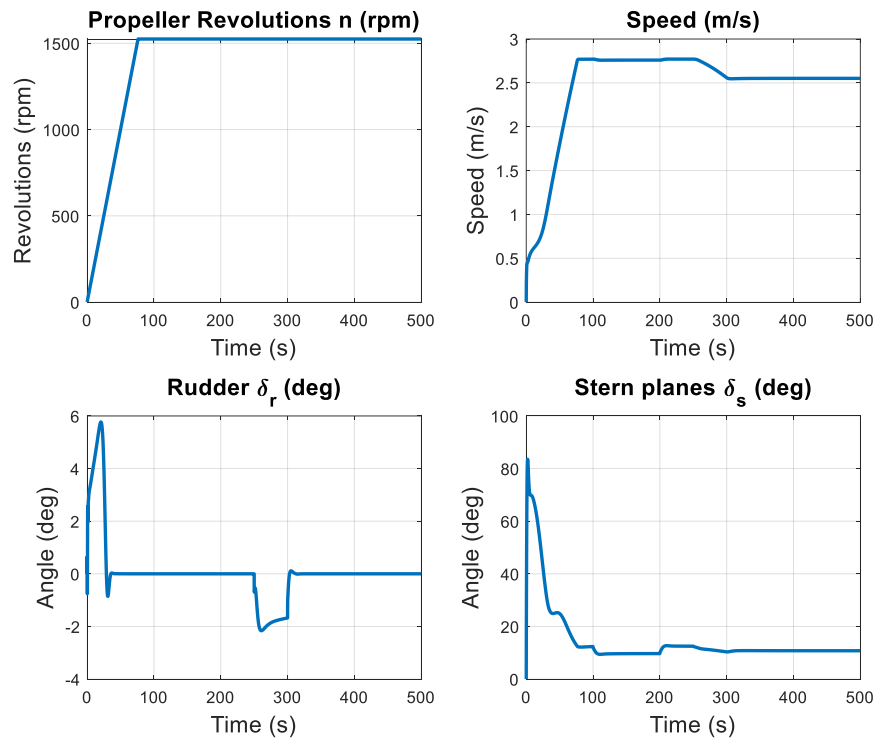
6.6 Trajectory 1, Non-Uniform Density

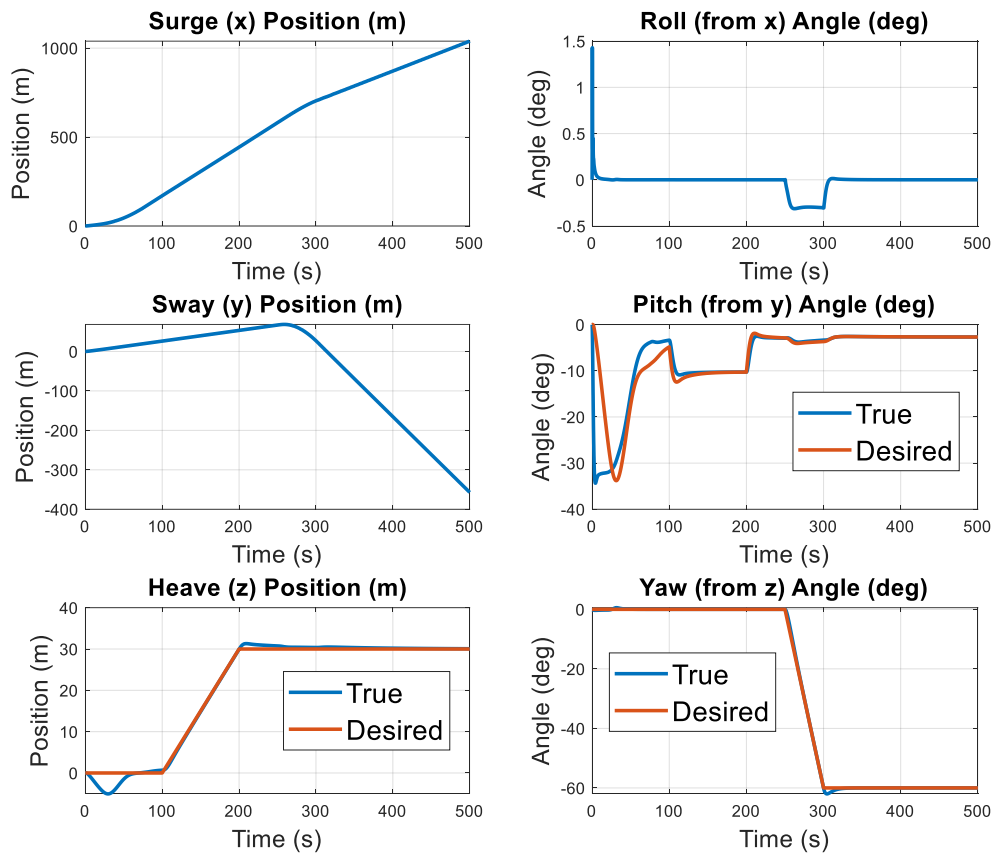
For the majority of our simulations, we looked at a vehicle with uniform density throughout. This is unrepresentative of a real AUV and a bit boring as it places the center of gravity at the centroid of the ellipsoid. The buoyancy force acts at the same point, with the same magnitude, in opposite directions of the gravitational force of vehicle causing the two to cancel out. In a real system we would likely see heavier components in the rear of the vehicle, the motor and fuel source (either battery or liquid fuel), with the lighter electronics used for the guidance control up front. To analyze the effects of a shift in the center of gravity, we considered a lighter uniform

density for the front 90% of the vehicle and a larger uniform density for the rear 10%, effectively shifting the center of gravity towards the rear.

We ran the simulation using our baseline input configuration: a sample time of .05 seconds, yaw angle trajectory 1, reasonable current speeds, and a fixed β angle. We compare the results of this simulation, Figure 17, to the results of the same system, but with constant density throughout, Figure 12.

The most notable observation is the initial dive in the pitch angle and the larger stern plane angle required to correct for it. This is known as the non-minimum phase effect and is observable in similar systems, such as aircraft, where the lack of a stiffness term in the plant model leads to a pole at zero in the s domain or one in the z domain. The added weight in the back of the vehicle turns its nose up initially, forcing the controller to compensate for it before it is able to track the desired profile. This sudden change in the pitch angle influences the heave position as well as the system needs to correct for the upward pointing noise before it is capable of diving to the desired depth.





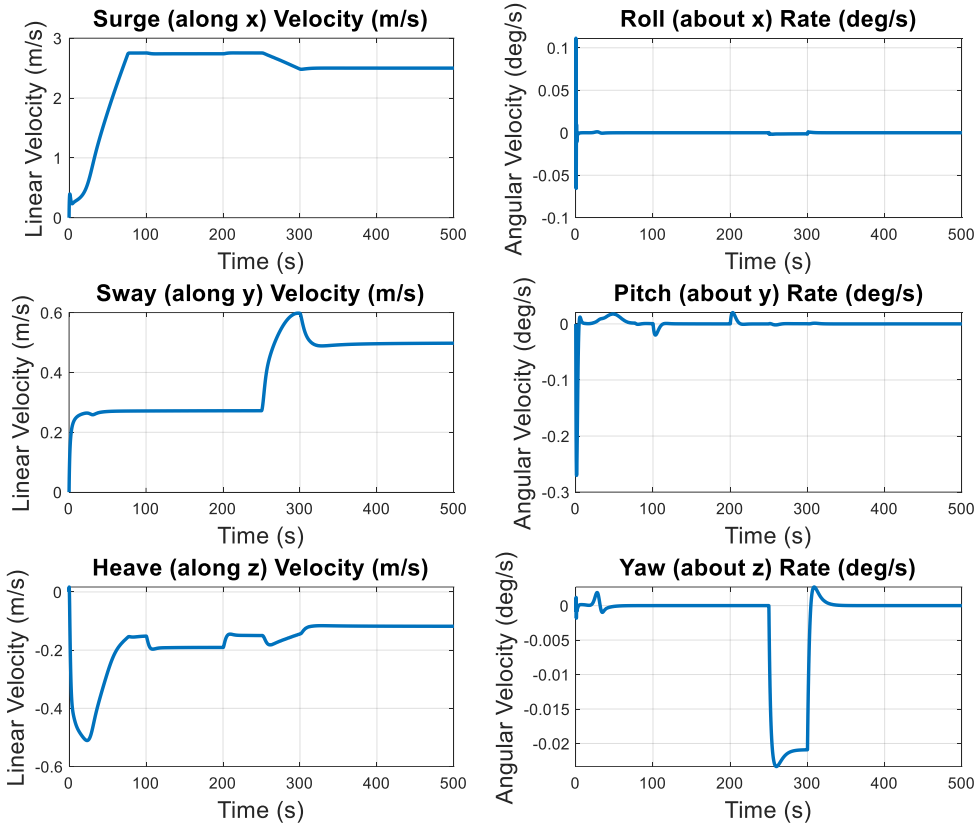


Figure 17: Nonuniform Density. Sampling time = .05 seconds (20 Hz), yaw trajectory 1, .5 m/sec current speed, fixed sideslip angle

7 Conclusions/Future Work

For this project a six degree of freedom, nonlinear plant model of the REMUS 100 AUV was successfully re-derived. The second order system was reduced to a first order system in the nonlinear state equations and the model was emulated in MATLAB.

The ability to track reference inputs for the three control inputs was demonstrated using discrete time PID controllers. It was shown that the controllers were able to track various yaw angle trajectories.

System robustness was demonstrated by evaluating the tracking capability for different current speed and horizontal angles of current flow.

In the future, additional work could be completed to further the results of this project. First, Lyapunov stability of the system could be investigated, referencing [1] for an in-depth discussion. The input profiles and disturbances could be expounded upon to include providing the inputs concurrently, as well as evaluating the effects of vertical current flow. Also, trajectories could be defined in terms of x and y coordinates in the NED frame and their

relationship modeled to the control inputs. For the control model, adaptive PID coefficients and optimal control methods could be investigated to further improve the model. Lastly, quantitative performance metrics could be defined in order to provide a more thorough parameter study.

8 References

- [1] Fossen, T. I. (2021). *Handbook of Marine Craft Hydrodynamics and Motion Control* (2nd ed.). Wiley.
- [2] Imlay, F. H. (1961). The Complete Expressions for Added Mass of a Rigid Body Moving in an Ideal Fluid. Technical Report DTMB 1528. David Taylor Model Basin. Washington D.C.
- [3] Beard, Randal W. and McLain, Timothy W. *Small Unmanned Aircraft: Theory and Practice*, Princeton: Princeton University Press, 2012.
- [4] “What Is an AUV?” *What Is an AUV? : Ocean Exploration Facts: NOAA Office of Ocean Exploration and Research*, <https://oceanexplorer.noaa.gov/facts/auv.html>.
- [5] “5 New Advancements in AUV Technology for Oil and Gas.” *Energy Digital*, 17 May 2020, <https://energydigital.com/utilities/5-new-advancements-auv-technology-oil-and-gas>.
- [6] Knight, Renee. “Militaries Are Taking Unmanned Underwater.” *Inside Unmanned Systems*, 28 Oct. 2021, <https://insideunmannedsystems.com/militaries-are-taking-unmanned-underwater/>.
- [7] A. Serrani and G. Conte, "Robust nonlinear motion control for AUVs," in *IEEE Robotics & Automation Magazine*, vol. 6, no. 2, pp. 33-38, June 1999, doi: 10.1109/100.774926.
- [8] L. Lapierre and B. Jouvencel, "Robust Nonlinear Path-Following Control of an AUV," in *IEEE Journal of Oceanic Engineering*, vol. 33, no. 2, pp. 89-102, April 2008, doi: 10.1109/JOE.2008.923554.
- [9] C. Shen, Y. Shi and B. Buckham, "Path-Following Control of an AUV: A Multiobjective Model Predictive Control Approach," in *IEEE Transactions on Control Systems Technology*, vol. 27, no. 3, pp. 1334-1342, May 2019, doi: 10.1109/TCST.2018.2789440.
- [10] “Ocean Current.” *Encyclopædia Britannica*, Encyclopædia Britannica, Inc., <https://www.britannica.com/science/ocean-current>.
- [11] US Department of Commerce, National Oceanic and Atmospheric Administration. “How Fast Is the Gulf Stream?” *NOAA’s National Ocean Service*, 1 June 2013, <https://oceanservice.noaa.gov/facts/gulfstreamspeed.html>.

Appendix A: Acronyms List

AUV	Autonomous underwater vehicle
B	Body reference frame

CO	Marine craft origin (origin of the body frame)
CG	Marine craft center of gravity
NED	North, East, Down inertial reference frame (N)

Appendix B: Variable List

x_b	Body frame longitudinal axis
y_b	Body frame transverse axis
z_b	Body frame normal axis
x_{flow}	Flow x-axis - axis parallel to freestream flow
y_{flow}	Flow y-axis
z_{flow}	Flow z-axis
$\vec{r}_{B/N}$	Vector relating body frame and inertial NED frame
$\vec{r}_{G/N}$	Vector relating CG of marine craft and inertial NED frame
\vec{r}_G	Vector relating CO and CG of marine craft
$R_x(\phi)$	General rotation matrix about x axis
$R_y(\theta)$	General rotation matrix about y axis
$R_z(\psi)$	General rotation matrix about z axis
R_B^N	Rotation matrix from body frame to NED
R_N^B	Rotation matrix from NED to body frame
$S(\lambda)$	Skew symmetric cross product operator
T_N^B	translation matrix from NED to body frame
β	Sideslip angle
α	Angle of attack
R_B^{Flo}	Rotation from body frame to flow frame
R_{Flow}^B	Rotation from flow frame to body frame
M_{RB}	rigid body mass matrix
v_G^B	generalized velocity vector
u	<i>Linear velocity in x</i>
v	<i>Linear velocity in y</i>
w	<i>Linear velocity in z</i>
p	<i>Angular velocity about x</i>
q	<i>Angular velocity about y</i>
r	<i>Angular velocity about z</i>
C_{RB}	rigid body Coriolis and centripetal matrix due to rotation of B about N
M_A	added mass matrix due to displacement of the surrounding fluid
v_{rel}^B	relative (to the ocean currents) velocity vector in the body frame
C_A	added Coriolis and centripetal matrix due to displacement of the surrounding fluid
D	linear damping matrix
g	gravitational and buoyancy forces and moments
η^N	generalized position vector in NED frame

x	<i>x Position</i>
y	<i>y Position</i>
z	<i>z Position</i>
ϕ	<i>Angle about x</i>
θ	<i>Angle about y</i>
ψ	<i>Angle about z</i>
τ_{Input}	control forces and moments
$\tau_{Current}$	forces and moments induced by the ocean currents
$\tau_{DragLift}$	hydrodynamic lift/drag forces
$\tau_{CrossFlowDrag}$	hydrodynamic cross flow drag terms
v_c^B	linear current expressed in the body frame
V_c	In the flow reference frame, the speed of the current
v_{rel}	Relative velocity (to ocean current) vector
v_G^B	linear velocity vector in the body frame
$\omega_{B/N}^B$	angular velocity vector of the body frame relative to the NED frame in the body frame
v_c^N	irrotational constant ocean current in the NED frame
a	Prolate spheroid radius along x axis
b	Prolate spheroid radius along y axis
c	Prolate spheroid radius along z axis
$\bar{x}, \bar{z}, \bar{y}$	Centroid coordinates of the AUV
$\bar{x}_{CG}, \bar{y}_{CG}, \bar{z}_{CG}$	Center of gravity coordinates of the AUV
I_G	Mass moment of inertia
F_B^N	buoyancy force which acts directly upwards in the NED frame at the center of buoyancy of the craft
F_G^N	gravitational force which acts directly downwards on the center of gravity of the craft in the NED frame
A	sum of the rigid body and added mass matrix
B	damping matrix
K	spring stiffness of hydrostatic matrix
ρ_{water}	Density of water
S	Shape of an object experiencing drag/lift
X_{Flow}	Flow direction
F_{drag}	Force of drag
F_{Lift}	Force of lift
C_D	Coefficient of drag
C_L	Coefficient of lift
AR	Aspect ratio
C_{D_0}	Initial drag coefficient
C_{D_α}	Drag coefficients dependence on angle of attack
C_{L_0}	Initial lift coefficient
C_{L_α}	Lift coefficients dependence on angle of attack
C_{D_p}	Parasitic drag coefficient

e	Eccentricity
$T(x)$	draft (in our case the diameter of the AUV)
v_r	relative linear velocity in the Y_B direction
w_r	relative linear velocity in the Z_B direction
r_r	relative angular velocity about the Z_B axis
$C_d^{2D}(x)$	cross flow drag coefficient that can be estimated using Hoerner's curve
Y_{rudder}	Rudder lift force perpendicular to $X_B Z_B$ plane in the Y_B direction
V_{rh}	relative speed in the horizontal plane
A_r	rudder area
C_{Lr}	rudder lift coefficient
δ_r	rudder angle
x_{rudder}	Rudder X_B position in the body frame
Z_{stern}	Stern plane lift force perpendicular to $X_B Y_B$ plane in Z_B direction
V_{rv}	relative speed in the vertical plane
A_s	stern plane area
C_{Ls}	stern lift coefficient
δ_s	stern plane angle
x_{stern}	Stern plane X_B position in the body frame
M	$(M_{RB} + M_A)$
C	$(C_A(v_{rel}^B) + C_{RB}(v_{rel}^B))$
τ_{Prop}	Propeller thrust force in the X_B direction
c_1, c_2, c_r, c_s	constants we identified from parameters in [1] associated with the motor model
V_{lin}	speed of the vehicle
θ_d	Desired pitch angle
$K_{p_z} K_{I_z}$	Depth controller PI coefficients
$K_{p_\theta} K_{D_\theta} K_{I_\theta}$	Pitch angle controller PID coefficients
$K_{p_\psi} K_{D_\psi} K_{I_\psi}$	Yaw angle controller PID coefficients

Appendix C: Miscellaneous Derivations

Centroid derivation

The centroid of a partial ellipsoid is given by Eqn. 4-6, \bar{x} can be found by as such

Cartesian coordinates will be used in the derivation of \bar{x} , therefore a small section of volume is $dV = \pi x z dx$

Start by solving for y and z using the cross sections of the ellipsoid

$$\frac{x^2}{a^2} + \frac{y^2}{b^2} = 1 \rightarrow y = \pm \sqrt{\frac{b^2}{a^2}(a^2 - x^2)} \quad \text{Eqn. C-1}$$

$$\frac{z^2}{c^2} + \frac{x^2}{a^2} = 1 \rightarrow z = \pm \sqrt{\frac{c^2}{a^2}(a^2 - x^2)} \quad \text{Eqn. C-2}$$

Using Eqn. C-1 and Eqn. C-2 the components of \bar{x} are solved below, \bar{x} is found from dividing the two

$$\int x \, dV = \pi \int_{LowBnd}^{UppBnd} x \frac{bc}{a^2} (a^2 - x^2) dx = \frac{bc\pi}{a^2} \left(\frac{a^2 x^2}{2} - \frac{x^4}{4} \right) \Big|_{LowBnd}^{UppBnd} \quad \text{Eqn. C-3}$$

$$\int dV = \pi \int_{LowBnd}^{UppBnd} \frac{bc}{a^2} (a^2 - x^2) dx = \frac{bc\pi}{a^2} \left(a^2 x - \frac{x^3}{3} \right) \Big|_{LowBnd}^{UppBnd} \quad \text{Eqn. C-4}$$

Derivation of the mass and centripetal matrices from conservation of linear and angular momentum

The time derivative in an inertial frame of a vector \vec{a} in a moving reference frame, such as the body frame satisfies

$$\frac{^I d}{dt} \vec{a} = \frac{^B d}{dt} \vec{a} + \vec{\omega}_{B/I} \times \vec{a} \quad \text{Eqn. C-5}$$

The distance from the origin of the NED frame to CG is represented by

$$\vec{r}_{G/N} = \vec{r}_{B/N} + \vec{r}_G \quad \text{Eqn. C-6}$$

By applying the relationship given by Eqn. C-5, the time derivative of $\vec{r}_{G/N}$ is

$$\vec{v}_{G/N} = \vec{v}_{B/N} + \left(\frac{^B d}{dt} \vec{r}_G + \vec{\omega}_{B/N} \times \vec{r}_G \right) \quad \text{Eqn. C-7}$$

For a rigid body, the time derivative of \vec{r}_G satisfies

$$\frac{^B d}{dt} \vec{r}_G = \vec{0} \quad \text{Eqn. C-8}$$

The conservation of linear momentum of CG is given by

$$\vec{f}_G = \frac{^N d}{dt} (m \vec{v}_{G/N}) = \frac{^B d}{dt} (m \vec{v}_{G/N}) + m \vec{\omega}_{B/N} \times \vec{v}_{G/N} \quad \text{Eqn. C-9}$$

The vectors in Eqn. C-9 can be expressed in the body frame, making the translation motion in CG equal to

$$m [\vec{v}_{G/N}^B + S(\vec{\omega}_{B/N}^B) \vec{v}_{G/N}^B] = \vec{f}_G^B \quad \text{Eqn. C-10}$$

where

$$S(\vec{\omega}_{B/N}^B) \vec{v}_{G/N}^B = \vec{\omega}_{B/N}^B \times \vec{v}_{G/N}^B$$

Similarly, it follows that the conservation of angular momentum of CG is

$$\begin{aligned}\vec{m}_G &= \frac{^N d}{dt} (I_G \vec{\omega}_{B/N}) = \frac{^B d}{dt} (I_G \vec{\omega}_{B/N}) + \vec{\omega}_{B/N} \times (I_G \vec{\omega}_{B/N}) \\ &= \frac{^B d}{dt} (I_G \vec{\omega}_{B/N}) - (I_G \vec{\omega}_{B/N}) \times \vec{\omega}_{B/N}\end{aligned}\quad \text{Eqn. C-11}$$

The vectors in Eqn. C-11 can be expressed in the body frame, making the rotational motion in CG equal to

$$\begin{aligned}I_G \dot{\omega}_{B/N}^B - S(I_G \omega_{B/N}^B) \omega_{B/N}^B &= m_G^B \\ \text{where } S(I_G \omega_{B/N}^B) \omega_{B/N}^B &= (I_G \omega_{B/N}^B) \times \omega_{B/N}^B\end{aligned}\quad \text{Eqn. C-12}$$

To transform the motion from CG to CO we derive the relationship between them as such, starting from Eqn. C-7 and Eqn. C-8

$$\begin{aligned}v_{G/N}^B &= v_{B/N}^B + \omega_{B/N}^B \times r_G^B \\ &= v_{B/N}^B - r_G^B \times \omega_{B/N}^B \\ &= v_{B/N}^B + S^T(r_G^B) \omega_{B/N}^B\end{aligned}\quad \text{Eqn. C-13}$$

Representing Eqn. C-13 in matrix form the transformation between the velocities of the two points $H(r_G^B)$ can be found

$$\begin{bmatrix} v_{G/N}^B \\ \omega_{B/N}^B \end{bmatrix} = \begin{bmatrix} I_{3x3} & S^T(r_G^B) \\ 0_{3x3} & I_{3x3} \end{bmatrix} \begin{bmatrix} v_{B/N}^B \\ \omega_{B/N}^B \end{bmatrix}\quad \text{Eqn. C-14}$$

where

$$H(r_G^B) = \begin{bmatrix} I_{3x3} & S^T(r_G^B) \\ 0_{3x3} & I_{3x3} \end{bmatrix}$$

Applying this transformation to Eqn. 4-8 yields the rigid body mass and Coriolis-centripetal matrices about CO

$$H^T(r_G^B) M_{RB}^{CG} H(r_G^B) \begin{bmatrix} \dot{v}_{B/N}^B \\ \dot{\omega}_{B/N}^B \end{bmatrix} + H^T(r_G^B) C_{RB}^{CG} H(r_G^B) \begin{bmatrix} v_{B/N}^B \\ \omega_{B/N}^B \end{bmatrix} = H^T(r_G^B) \begin{bmatrix} f_G^B \\ m_G^B \end{bmatrix}$$

where

$$M_{RB}^{CO} = H^T(r_G^B) M_{RB}^{CG} H(r_G^B) = \begin{bmatrix} mI_{3x3} & -mS(r_G^B) \\ mS(r_G^B) & I_G - mS^2(r_G^B) \end{bmatrix}\quad \text{Eqn. C-15}$$

and

$$= \begin{bmatrix} mS(\omega_{B/N}^B) & -mS(\omega_{B/N}^B)S(r_G^B) \\ mS(r_G^B)S(\omega_{B/N}^B) & mS(r_G^B)S(\omega_{B/N}^B)S^T(r_G^B) - S(I_G \omega_{B/N}^B) \end{bmatrix}$$

Derivation of the mass moment of inertia matrix terms

The mass moments of inertia matrix is given by Eqn. 4-10, where

$$I_x = \int_V (y^2 + z^2) \rho dV, \quad I_y = \int_V (x^2 + z^2) \rho dV, \quad I_z = \int_V (x^2 + y^2) \rho dV \quad \text{Eqn. C-16}$$

$$I_{xy} = I_{yx} = \int_V xy \rho dV, \quad I_{xz} = I_{zx} = \int_V xz \rho dV, \quad I_{yz} = I_{zy} = \int_V yz \rho dV$$

To compute these terms for a partial prolate spheroid about the body frame (with the center of the spheroid located at the origin of the body frame as shown in Figure 5) start by representing the equation of an ellipsoid in cylindrical coordinates

$$\frac{x^2}{a^2} + \frac{y^2}{b^2} + \frac{z^2}{c^2} = 1$$

Let

$$y = b \cdot r \cos \theta, \quad z = c \cdot r \sin \theta, \quad z_{cyl} = a \cdot x \quad \rightarrow r^2 + z^2 = 1 \quad \text{Eqn. C-17}$$

where

$$0 \leq r \leq \sqrt{1 - z_{cyl}^2}, \quad 0 \leq \theta \leq 2\pi, \quad -1 \leq z_{cyl} \leq 1$$

The components that make up the individual mass moment of inertia terms can be solved for independently and summed together because the integral is a linear operator. In cylindrical coordinates $dV = a \cdot b \cdot c \cdot r dr d\theta dz$

$$\begin{aligned} \int_V x^2 dV &= a^3 bc \int_{LowBnd}^{UppBnd} \int_0^{2\pi} \int_0^{\sqrt{1-z^2}} z^2 r dr d\theta dz \\ &= a^3 bc \int_{LowBnd}^{UppBnd} \int_0^{2\pi} \frac{1}{2} (z^2 - z^4) d\theta dz \\ &= a^3 bc \int_{LowerBnd}^{UppBnd} \pi (z^2 - z^4) dz \\ &= a^3 bc \pi \left(\frac{z^3}{3} - \frac{z^5}{5} \right) \Big|_{LowBnd}^{UppBnd} \end{aligned} \quad \text{Eqn. C-18}$$

$$\begin{aligned} \int_V y^2 dV &= ab^3 c \int_{LowBnd}^{UppBnd} \int_0^{2\pi} \int_0^{\sqrt{1-z^2}} r^3 \cos^2 \theta dr d\theta dz \\ &= ab^3 c \int_{LowBnd}^{UppBnd} \int_0^{2\pi} \frac{1}{4} (1 - z^2)^2 \cos^2 \theta d\theta dz \\ &= ab^3 c \int_{LowerBnd}^{UppBnd} \frac{\pi}{4} (1 - z^2)^2 dz \\ &= ab^3 c \frac{\pi}{4} \left(\frac{z^5}{5} - \frac{2z^3}{3} + z \right) \Big|_{LowBnd}^{UppBnd} \end{aligned} \quad \text{Eqn. C-19}$$

$$\begin{aligned}
\int_V z^2 dV &= abc^3 \int_{LowBnd}^{UppBnd} \int_0^{2\pi} \int_0^{\sqrt{1-z^2}} r^3 \sin^2 \theta dr d\theta dz \\
&= abc^3 \int_{LowBnd}^{UppBnd} \int_0^{2\pi} \frac{1}{4} (1-z^2)^2 \sin^2 \theta d\theta dz \\
&= abc^3 \int_{LowerBnd}^{UppBnd} \frac{\pi}{4} (1-z^2)^2 dz \\
&= abc^3 \left. \frac{\pi}{4} \left(\frac{z^5}{5} - \frac{2z^3}{3} + z \right) \right|_{LowBnd}^{UppBnd}
\end{aligned} \tag{Eqn. C-20}$$

$$\int_V xy dV = a^2 b^2 c \int_{LowBnd}^{UppBnd} \int_0^{2\pi} \int_0^{\sqrt{1-z^2}} rz \cos \theta dr d\theta dz = 0 \tag{Eqn. C-21}$$

$$\int_V yz dV = ab^2 c^2 \int_{LowBnd}^{UppBnd} \int_0^{2\pi} \int_0^{\sqrt{1-z^2}} r^2 \cos \theta \sin \theta dr d\theta dz = 0 \tag{Eqn. C-22}$$

$$\int_V xz dV = a^2 bc^2 \int_{LowBnd}^{UppBnd} \int_0^{2\pi} \int_0^{\sqrt{1-z^2}} rz \sin \theta dr d\theta dz = 0 \tag{Eqn. C-23}$$

Total inertia of the spheroid is the sum of its parts, this is found using the parallel axis theorem

$$I_g = \sum (I_{R,i} - m_i S^2(r_{R,i}^{CG})) \tag{Eqn. C-24}$$

Coriolis-Centripetal matrix as a function of mass matrix derivation

The Coriolis-centripetal mass matrix can be expressed in terms of the rigid body mass matrix.

Consider kinetic energy T written in quadratic form:

$$T = \frac{1}{2} v^T M v, \quad M = M^T > 0$$

where

$$M = \begin{bmatrix} M_{11} & M_{12} \\ M_{21} & M_{22} \end{bmatrix} \tag{Eqn. C-25}$$

expanded

$$\rightarrow T = \frac{1}{2} (v_1^T M_{11} v_1 + v_1^T M_{12} v_2 + v_2^T M_{21} v_1 + v_2^T M_{22} v_2)$$

It follows from Kirchhoff's equations, which represent the motion of a rigid body in an ideal fluid

$$\frac{d}{dt} \left(\frac{\partial T}{\partial v_1} \right) + S(v_2) \frac{\partial T}{\partial v_1} = \tau_1 \tag{Eqn. C-26}$$

$$\frac{d}{dt} \left(\frac{\partial T}{\partial v_2} \right) + S(v_2) \frac{\partial T}{\partial v_2} + S(v_1) \frac{\partial T}{\partial v_1} = \tau_2$$

Plug in Eqn. C-25 Eqn. C-26 and removing the terms dependent on acceleration leaves the terms that are due to Coriolis-centripetal forces

$$C(v)v = \begin{bmatrix} S(v_2) \frac{\partial T}{\partial v_1} \\ S(v_2) \frac{\partial T}{\partial v_2} + S(v_1) \frac{\partial T}{\partial v_1} \end{bmatrix} = \begin{bmatrix} 0_{3x3} & -S \left(\frac{\partial T}{\partial v_1} \right) \\ -S \left(\frac{\partial T}{\partial v_1} \right) & -S \left(\frac{\partial T}{\partial v_2} \right) \end{bmatrix} \begin{bmatrix} v_1 \\ v_2 \end{bmatrix} \quad \text{Eqn. C-27}$$

Using the derivative of the quadratic form

$$\frac{\partial}{\partial x} (x^T A x) = Ax + A^T x \quad \text{Eqn. C-28}$$

And the knowledge that the components of the mass matrix are symmetric

$$M_{12} = {M_{21}}^T, \quad M_{21} = {M_{12}}^T \quad \text{Eqn. C-29}$$

The partials of kinetic energy with respect to the velocity components are

$$\begin{aligned} \frac{\partial T}{\partial v_1} &= M_{11}v_1 + M_{12}v_2 \\ \frac{\partial T}{\partial v_2} &= M_{21}v_1 + M_{22}v_2 \end{aligned} \quad \text{Eqn. C-30}$$

Eqn. C-27 can be manipulated to the form

$$C(v)v = \begin{bmatrix} 0_{3x3} & -S(M_{11}v_1 + M_{12}v_2) \\ -S(M_{11}v_1 + M_{12}v_2) & -S(M_{21}v_1 + M_{22}v_2) \end{bmatrix} \begin{bmatrix} v_1 \\ v_2 \end{bmatrix} \quad \text{Eqn. C-31}$$